Atmos. Chem. Phys. Discuss., 10, 15811–15884, 2010
www.atmos-chem-phys-discuss.net/10/15811/2010/
doi:10.5194/acpd-10-15811-2010

Atmospheric Chemistry and Physics Discussions

Modeling natural emissions in the Community Multiscale Air Quality (CMAQ) model – Part 2: Modifications for simulating natural emissions

S. F. Mueller, Q. Mao, and J. W. Mallard

Tennessee Valley Authority, P.O. Box 1010, Muscle Shoals, Alabama 35662-1010, USA

Received: 28 May 2010 – Accepted: 7 June 2010 – Published: 28 June 2010

Correspondence to: S. F. Mueller (sfmueller@tva.gov)

Published by Copernicus Publications on behalf of the European Geosciences Union.

Abstract

A recent version (4.6) of the Community Multiscale Air Quality (CMAQ) model was used as the basis for testing model revisions for including reactions involving chlorine (HCl, $ClNO_2$) and reduced sulfur (dimethylsulfide, or DMS, and H_2S) species not normally treated in the CB05 gas chemical mechanism and cloud chemistry module. Model chemistry revisions were based on published reaction kinetic data and a recent cloud chemistry model that includes heterogeneous reactions of organic sulfur compounds. Testing of the revised model was conducted using a recently enhanced data base of natural emissions that includes ocean and continental sources of DMS, H_2S, chlorinated gases and lightning NO_x for the continental United States and surrounding regions. Results using 2002 meteorology and emissions indicated that most simulated chemical and aerosol species exhibit the expected seasonal variations in grid-average surface concentrations. Ozone exhibits a winter and early spring maximum – reasonably consistent with ozone data and model results produced by others – in a pattern that reflects the influences of atmospheric dynamics and pollutant background levels imposed on the CMAQ simulation by boundary conditions derived from a global model. A series of experimental model simulations reveals that the addition of gas phase organic sulfur chemistry leads to sulfate aerosol increases over most of the continental United States. Modifications to the cloud chemistry module result in widespread decreases in SO_2 across the modeling domain and a mix of sulfate increases and decreases. Most cloud-mediated sulfate increases occurred over the Pacific Ocean (up to about 0.1 $\mu g\, m^{-3}$) and at slightly lesser amounts over and downwind from the Gulf of Mexico (including portions of the Eastern US). Variations in the chemical response are due to the link between DMS/H_2S and their byproduct SO_2, the heterogeneity of cloud cover and precipitation (precipitating clouds act as net sinks for SO_2 and sulfate), and the persistence of cloud cover (the largest relative sulfate increases occurred over the persistently cloudy Gulf of Mexico and western Atlantic Ocean). Overall, the addition of organic sulfur chemistry increased surface hourly sulfate levels by as much as

ACPD
10, 15811–15884, 2010

1–2 $\mu g\, m^{-3}$ in selected grid cells. The added chemistry produced significantly less sulfate in the vicinity of high SO_2 emissions (e.g., wildfires), perhaps in response to lower OH from competing reactions with DMS and its derivatives. Simulated surface levels of DMS compare favorably with published observations made in the marine boundary layer. However, DMS derivatives are lower than observed implying either less chemical reactivity in the model or a low bias in the boundary conditions for DMS derivatives such as dimethylsulfoxide. The sensitivity of sulfate to cloud cover and the aqueous sulfate radical is also explored. This revised version of CMAQ provides a tool for more realistically evaluating the influence of natural emissions on air quality.

1 Introduction

A companion paper (Smith and Mueller, 2010) describes development of an expanded natural emissions data set for use in the United States Environmental Protection Agency (EPA) Community Multiscale Air Quality (CMAQ) Model. The rationale for doing so is the need for scientifically defensible estimates of naturally occurring levels of air pollutants. Natural contributions to air pollution play an important role in determining overall human and ecosystem exposures to potentially damaging pollutants, and set limits to and benchmarks for the pollutant reduction objectives at the heart of air pollution policy and regulations. Examples of the importance placed on naturally occurring pollutants include the guidelines for implementing the Regional Haze Rule (EPA, 2003), and the interest in background pollutant levels for their potential impact on achieving air quality standards (Lin et al., 2000; EPA, 2005).

This paper describes modifications in the CMAQ Model required so that it can fully use the natural emissions data developed by Smith and Mueller (2010). CMAQ is a widely used tool for estimating the association between pollutant emissions and downwind ambient concentrations. The most significant model changes were those needed to incorporate chemical reactions for organic sulfur compounds and associated reactive species in both the gas and aqueous (cloud) phases. The result is a model that

ACPD
10, 15811–15884, 2010

simulates the spatial and temporal variability in naturally-occurring ozone, fine particles and acid deposition. Tests of the revised model are described to illustrate the effects of the modified chemistry on simulated air quality. Work is underway to document more extensive simulations of the revised model and to provide insight into the contributions of different natural phenomena to air pollutant levels.

2 Previous work

2.1 Current treatment of natural emissions in CMAQ

This study used version 4.6 of the CMAQ model (CMAQ4.6 released October 2006) to examine natural levels of ozone and airborne particles. The EPA Models-3 air quality modeling system – including the SMOKE emissions and CMAQ air quality components – has long treated pollutant emissions from natural processes and systems (as distinguished from those that are created by human activity): (1) biogenic emissions of volatile organic compounds (VOCs) emitted by vegetation; (2) NO emissions from soils; (3) emissions from wildfires; (4) windblown dust; (5) animal-derived NH_3. Recently, changes implemented in CMAQ4.6 enable internal computation of sea salt particle emissions. Thus, the SMOKE/CMAQ4.6 modeling system treats many primary particulate emissions and some ozone and secondary fine particle ($PM_{2.5}$, or particles <2.5 µm in size) precursor emissions.

2.2 Additions made to the standard SMOKE/CMAQ suite of natural emissions

Berntsen and Isaksen (1997) modeled global tropospheric photochemistry based on the Global Emissions Inventory Activity (GEIA) emissions data base (http://www.geiacenter.org/). This data base includes both anthropogenic and natural emissions, the latter including fluxes from biomass burning, biogenic sources (vegetation VOCs and soil NO), lightning NO_x (LNO_x) and oceans [dimethylsulfide (DMS), NH_3, HCl and

ACPD
10, 15811–15884, 2010

$ClNO_2$]. However, given the focus of Berntsen and Isaksen (1997) on ozone it is not clear to what extent their modeling used all the emissions species that are currently available.

Park et al. (2004) used GEOS-Chem to simulate atmospheric aerosols derived in part from natural sulfur emissions from oceans (DMS), volcanoes, NO_x from lightning, vegetation, and soils, biomass burning emissions (including CO, NO_x and VOCs), and ammonia emitted by animals. Likewise, Kaminski et al. (2007) used data from the EDGAR 2.0 and GEIA emissions inventories for their global air quality modeling effort including emissions from these same sources. They incorporated monthly mean totals of LNO_x from the GEIA data base, scaling emission horizontally according to the modeled distribution of convective clouds and vertically following profiles reported by Pickering et al. (1993).

Koo et al. (2010) recently examined potential air quality impacts of selected natural emissions not normally treated in the CMAQ Model. They added lightning NO_x and surrogates for organosulfur from oceans. Their approach to estimating LNO_x emissions started with an annual estimate to total LNO_x emitted across the United States followed by a spatial-temporal allocation scheme based on simulated convective precipitation. Organosulfur species DMS and methanesulfonic acid (MSA) were treated using ocean emissions estimates from the global GEOS-Chem model, and by using SO_2 as a surrogate for DMS and sulfate as a surrogate for MSA. This approach avoided the need for modifying the model chemistry but leaves questions about the validity of such an assumption. Koo et al. (2010) concluded that LNO_x contributes significantly (1–6 ppbV) to annual average ozone levels, especially across the southeastern US. They also determined that their scheme for estimating organosulfur pollutants decreased ozone slightly (due to the added sulfur reacting with OH) in the vicinity of the emissions and increased fine particle mass by amounts generally $<0.25\,\mu g\,m^{-3}$ on an annual average.

It is clear from the work cited here that there are natural emissions not treated in the standard SMOKE/CMAQ modeling package that are considered important on regional and global scales. Most notably, these emissions involve reduced sulfur (especially

ACPD
10, 15811–15884, 2010

DMS), NH_3 and soluble chlorine species from oceans, and LNO_x. Despite the inherent uncertainty in quantifying these emissions, it is imperative to include them in any effort to examine a more complete picture of how natural emissions influence air quality. Smith and Mueller (2010) describe in detail the methodologies used to add natural emissions to the standard SMOKE/CMAQ inventory. Data from the National Lightning Detection Network along with recent work estimating NO_x production from lightning strokes formed the basis of LNO_x emission estimates. Ammonia emissions from populations of large wild animals were included using estimates from US and Canadian wildlife inventories and emissions estimates for Mexico in the GEIA data base. Atmospheric chlorine is believed to play a role in ozone formation in coastal areas (Knipping and Dabdub, 2003) and provides radicals that may also contribute to aerosol formation in clouds. Effective emissions rates for HCl and $ClNO_2$ in the marine boundary layer were incorporated from the GEIA data base, as were ammonia emissions from the oceans.

Reduced sulfur emissions from oceans and geogenic sources are also overlooked in CMAQ. Emissions of DMS, and to a lesser extent H_2S, are considered an important source of marine aerosols (Kreidenweis et al., 1991). Though relatively small compared to the oceans, inland lakes and coastal wetlands are also important sources of DMS and H_2S (National Acid Precipitation Assessment Program, 1991). Geogenic sources – especially the thermal vents of geologically active regions like Yellowstone National Park – emit H_2S that may be important contributors to downwind aerosols. Emissions from volcanoes were generally not included due to the sporadic nature of their emissions.

3 CMAQ modifications

Version 4.6 was the most recent release of CMAQ at the outset of this project. Because CMAQ is updated every 1–2 years it is impractical to try keeping up to date with the most current version, especially when independent model changes require

ACPD
10, 15811–15884, 2010

extensive testing. This study focused solely on version 4.6 although a more recent version (4.7) has since been released. A consequence of frequent code updates is that a more recent version often contains additional features or improvements that require further changes to ongoing work. Version 4.7 includes updates to the gas phase chemical mechanism that would have made unnecessary most of the chlorine reaction additions described later in this section. Also, CMAQ4.7 includes additional cloud chemistry reactions that enable some heterogeneous formation of organic aerosols. These reactions were not included in the current work but can easily be incorporated in the revised cloud chemistry module described below. Finally, secondary organic aerosol (SOA) formation in CMAQ4.6 (originally introduced into version 4.5.2) was updated from that in the original model version based on Morris et al. (2006) and further described in Sect. 4.1. It is important to note that the SOA treatment in CMAQ4.7 is somewhat different from that in CMAQ4.6.

3.1 Gas phase chemistry

This work uses the CMAQ optional configuration that includes an updated version of the carbon bond IV (CBIV) chemical mechanism called "CB05" (Yarwood et al., 2005). Changes made to the CMAQ4.6 CB05 gas phase chemical mechanism fall into three categories: (1) reactions added to treat chlorine species and/or involving chlorine radicals, (2) reactions added to treat DMS and its derivatives, and (3) reactions added to treat H_2S and its derivatives.

3.1.1 Chlorine reactions from CMAQ CBIV

Emissions of species HCl and $ClNO_2$ (nitryl chloride) require that gas- and aqueous-phase reactions be added that treat various chlorine species and their derivatives. CMAQ4.6 has an option to include a set of chlorine reactions in CB05, but it also includes reactions involving hazardous air pollutants (http://www.cmascenter.org/help/model_docs/cmaq/4.6/HAZARDOUS_AIR_POLLUTANTS.txt). This CB05 enhance-

ACPD
10, 15811–15884, 2010

ment was not used here because it required carrying a number of reactions that are not of interest for simulating natural ozone and aerosols. Instead, a subset of chlorine reactions originally added to the CMAQ4.6 CBIV reaction set were copied for use in CB05. This set of reactions (except for the last one), originally developed by Tanaka and Allen (2001), is listed in Table 1. These reactions produce radicals (Cl, ClO, OH, HO_2, XO_2) that react with VOCs, NO, H_2S, DMS and their oxidation products, and can play an important role in the chemistry of ocean coastal environments.

3.1.2 Nitryl chloride

Nighttime reactions of N_2O_5 on sea salt aerosols release $ClNO_2$ (Behnke et al., 1997) while other reactions involving sea salt aerosols release chlorine gas and HCl (Knipping and Dabdub, 2003). Chlorine gas photolyzes to atomic chlorine and $ClNO_2$ reacts with OH to form HOCl and NO_2. Thus, $ClNO_2$ is a reservoir of NO_2 in the marine boundary layer and provides reactive HOCl which further photolyzes to OH and Cl. Nitryl chloride is produced at levels roughly 100 times less than HCl (Erickson et al., 1999) and ambient concentrations of Cl are extremely low except in areas affected by anthropogenic chlorine and/or NO_x emissions. Treating the dechlorination of sea salt aerosol explicitly in CMAQ requires a modification to the aerosol module and was beyond the scope of this project. Instead, we added $ClNO_2$ as an emitted species from the ocean following data provided in the GEIA global emissions data base (Graedel et al., 1993; Erickson et al., 1999). One reaction added to the Tanaka and Allen (2001) chlorine reaction set was

$$OH + ClNO_2 \rightarrow HOCl + NO_2 \quad \text{(R1)}$$

as presented in Atkinson et al. (2007). Note that HCl can be an important contributor to cloud droplet acidity in the marine environment. Also, aqueous Cl^- plays a role in the droplet balance of various chlorine species that react with different organic sulfur species. Details of the heterogeneous chemistry modifications are provided in Sect. 3.2.

ACPD
10, 15811–15884, 2010

3.1.3 H_2S

Inorganic sulfur reactions added to CMAQ CB05 are listed in Table 2. Kinetic data exist for reactions of H_2S with OH, O, HO_2, Cl and NO_3. Each of the OH, O and Cl radicals is known to attack the S bond with H and produce the SH radical. Both HO_2 and NO_3 are likely to act similarly on H_2S although their reaction products have not been directly identified. The rate constant for H_2S+Cl has been measured to be the highest (7.4×10^{-11} cm^3 molecule^{-1} s^{-1} at 298 K) of this set of reactions. The next highest rate constants are for reactions involving OH and O (at 298 K): $k\approx5\times10^{-12}$ cm^3 molecule^{-1} s^{-1} for the OH reaction is about two orders of magnitude greater than that for the O reaction (NASA, 1997). Upper limits to the rate constants for the reactions involving HO_2 and NO_3 are both $\sim1\times10^{-15}$ cm^3 molecule^{-1} s^{-1} (Atkinson et al., 2004). During daytime, the reaction of H_2S with OH will dominate over that with O, while the reaction with Cl could be important over the ocean and in the presence of chlorine emissions. At night, the reaction with NO_3 will most likely be the dominant pathway for initiating the breakdown of H_2S with assumed products (by analogy with the other reactions) of SH and nitric acid. The reactions of H_2S with Cl, OH and NO_3 were added to the CB05 mechanism.

SH Reactions: The second step in oxidizing H_2S in the atmosphere involves reactions of SH with a variety of species. Data exist on the kinetics of SH reactions with O, O_2, O_3, NO, NO_2, Cl_2 and H_2O_2, as well as various bromine and fluorine species (NASA, 1997). At 298 K, rate constants k_i for SH reactions with species i are as follows (all have units of cm^3 molecule^{-1} s^{-1}): $k_O=1.6\times10^{-10}$; $k_{O_2}<4\times10^{-19}$; $k_{O_3}=3.7\times10^{-12}$; $k_{NO_2}=6.5\times10^{-11}$; $k_{Cl_2}=1.7\times10^{-10}$; $k_{H_2O_2}<5\times10^{-15}$. The reaction SH+NO+M has a more complex rate constant expression that is a function of altitude (pressure) in the atmosphere. At sea level and 298 K $k_{NO}=2.6\times10^{-12}$ cm^3 molecule^{-1} s^{-1}. The slowest reaction is by far SH+O_2, but the abundance of O_2 as a reactant makes it competitive with most other trace species as an important pathway for SH removal. The reaction with H_2O_2 appears to be the least important overall and was dropped from consid-

ACPD
10, 15811–15884, 2010

eration (note that Friedl et al., 1985, reported finding little net production of product species HSO from this reaction). Reactions involving NO and NO_2 will be important only downwind of NO_x emission sources. SH reactions with O and O_2 produce the SO radical whereas reaction with O_3 and NO_2 produce HSO. Reaction with NO produces HSNO and reaction with Cl_2 produces ClSH. Both HSNO and ClSH are treated as termination products.

SO Reactions: Data on reactions of SO with OH, O_2, O_3, NO_2 and ClO have been reported and all produce SO_2 (NASA, 1997). The reaction with O_2 is the slowest, but the abundance of O_2 makes it important relative to the other reactions. ClO is a product of the reaction between Cl and O_3. All of these reactions are included in the revision to CB05.

HSO Reactions: Atkinson et al. (2004) report kinetic rate constants for HSO reactions with O_2, O_3, NO and NO_2. As with other species, the reaction with O_2 is the slowest but the abundance of atmospheric O_2 makes it important. HSO reacting with NO is also very slow compared to the other reactions and was not included in this version of CB05. The reaction of HSO+NO_2 may produce HSO_2+NO (NASA, 1997) and these products were adopted for use here. HSO reacting with O_2 and O_3 are assumed to produce HSO_2 by analogy with the products of the NO_2 reaction. The only reaction identified for removing HSO_2 is that with O_2, but it is fairly rapid given the levels of O_2.

3.1.4 DMS and its derivatives

A realistic treatment of organic sulfur compounds must consider reactions between them and the various radicals present in the atmosphere. This is especially important in the case where "natural" pollutants are combined with anthropogenic pollutants because all pollutant reactions must compete for the available radicals. Finlayson-Pitts and Pitts (2000) provide a detailed overview of organic sulfur chemistry in the atmosphere. There is still much that needs to be learned about the reaction kinetics and reaction products that are involved. However, the level of detail described in the Finlayson-Pitts and Pitts (2000) overview is sufficient for constructing a treatment

ACPD
10, 15811–15884, 2010

of DMS+products chemistry. Reactions added to CB05 are generally only those for which the products and kinetic rates are known and are sufficiently fast that they will have a significant impact on the evolution of atmospheric sulfur. Consideration was given to include those reactions that, although slow in comparison to competing daytime reactions, would be relatively important at night.

Table 3 lists the reactions added to CB05. Unless otherwise noted, details of reaction kinetics were taken from NASA (1997) and Atkinson et al. (2004). Reactions of DMS with various atmospheric constituents have been studied extensively because of the suspected role of DMS in aerosol formation and climate. A great deal has been learned within the past 10 years. The evolution of DMS in the atmosphere as described by Finlayson-Pitts and Pitts (2000) and as simulated in previous models was followed as a road map for modifying the CMAQ4.6 CB05 mechanism. Uncertainties in the chemistry of DMS and its byproducts are described in this section. Compromises and assumptions were necessary to treat some of the reactions and/or byproducts due to incomplete knowledge and the various assumptions are explained.

DMS reactions: Studies of DMS chemistry have revealed that it is relatively reactive with a broad spectrum of chemical species, including O_3, OH, HO_2, O, Cl, ClO, IO, BrO, F, NO_3, and N_2O_5. Halogen species are most likely to be found in the marine boundary layer. Ubiquitous O_3 would play an important role if its reaction rate was not so slow (rate constant $k<1\times10^{-18}$ cm^3 molecule^{-1} s^{-1}). A comparative analysis of the various reactions revealed that DMS reactions with O, Cl, OH, OH+O_2, and NO_3 were most likely to control the fate of DMS in the atmosphere. Reactions with other halogen compounds are probably also important in selected situations but little is known about naturally occurring emissions and atmospheric levels of species like IO and BrO. Reactions involving halogen species other than chlorine were not treated at this time to avoid guesswork about their emissions.

The fastest reaction considered was DMS+Cl. This reaction occurs by way of two channels with a rate constant of about 3.3×10^{-10} cm^3 molecule^{-1} s^{-1} at 298 K (mea-

ACPD
10, 15811–15884, 2010

sured near 1 atm):

$$Cl + CH_3SCH_3 \rightarrow HCl + CH_3SCH_2 \quad (R2)$$

$$\rightarrow CH_3S(Cl)CH_3 \quad (R3)$$

Finlayson-Pitts and Pitts (2000) report that although both channels appear to be equally important, the fate of the adduct $CH_3S(Cl)CH_3$ is unknown. Thus, only (R2) is included in CMAQ.

The reaction of OH with DMS is perhaps the most studied of all reactions involving DMS and it is one of the most complex. As with chlorine, the reaction occurs by way of two reaction channels:

$$OH + CH_3SCH_3 \rightarrow CH_3SCH_2 + H_2O \quad (R4)$$

$$OH + CH_3SCH_3 + M \leftrightarrow CH_3S(OH)CH_3 + M \quad (R5)$$

At 298 K and 1 atm (R4) is predominant but the (R5) becomes more important as temperature decreases. The OH adduct itself may decompose back to its original reactants or it can react with O_2 to form dimethylsulfoxide (DMSO):

$$CH_3S(OH)CH_3 + O_2 \rightarrow CH_3SOCH_3 + HO_2 \quad (R6)$$

DMSO reacts rapidly with O_2 to form dimethylsulfone [DMSO2: $CH_3S(O)(O)CH_3$]. In addition, CH_3SCH_2 ($MSCH_2$) reacts with O_2 as

$$CH_3SCH_2 + O_2 + M \rightarrow CH_3SCH_2OO + M \quad (R7)$$

to form the peroxyl radical CH_3SCH_2OO (MSP).

The CMAQ CB05 mechanism revision includes both (R6) and (R7). The first channel is modeled following Atkinson et al. (2004) with the product $MSCH_2$ treated explicitly along with its subsequent reaction to MSP. The chain of reactions that begins with formation of the OH adduct (by way of the second DMS+OH channel) is modeled following Zhu et al. (2006):

$$DMS + OH + O_2 \rightarrow 0.5DMSO + 0.2DMSO2 + 0.3MSIA \quad (R8)$$

ACPD
10, 15811–15884, 2010

where MSIA is methanesulfinic acid.

Another reaction treated in the revised CB05 is DMS+O which yields CH_3SO and a methyl radical (Atkinson et al., 2004). The final DMS reaction treated here, important at night, is DMS+NO_3. This reaction yields MSCH2 and nitric acid.

$MSCH_2$ Reactions: This radical is formed by three of the five DMS reactions. Its primary reaction pathways are with O_2 and NO_3. The reaction with O_2 is very rapid and produces the peroxyl radical MSP. Products of $MSCH_2$+NO_3 are not known and are assumed, analogous to the companion reaction with O_2, to be MSP and NO.

MSP Reactions: This mechanism includes three reactions involving MSP as a reactant. One is the reaction of MSP with itself. The other two are MSP with NO and MSP with HO_2. MSP reactions with itself and other species are believed to form CH_3SCH_2O which is very unstable and rapidly decomposes to CH_3S and HCHO. Thus, all reactions involving MSP are treated as yielding products CH_3S, HCHO and, in the case of MSP+NO, NO_2.

CH_3S Reactions: Finlayson-Pitts and Pitts (2000) report that the fate of CH_3S in the atmosphere is unclear. This is because there is evidence that it reacts with many different species in a variety of ways and in most cases the products are not well known. For example, CH_3S+O_2 produces CH_3SOO, but the latter has a short lifetime because it decomposes back to CH_3S. Reaction with NO_2 produces CH_3SO+NO. CH_3S+O_3 is another likely reaction but a large number of potential reaction channels exist. These include yields of CH_3SO+O_2 (the yield is low at low pressure while data at high pressure are nonexistent), CH_3+SO+O_2, CH_2SO+H+O_2, CH_2SO+HO_2, CH_2S+OH+O_2, and CH_3O+SO_2. The percent yields of many of these channels are estimated to be very small and species like CH_2SO and CH_2S are very short-lived. Consequently, Zhu et al. (2006) aggregated several reactions into a single net reaction for CH_3S with a host of ambient species as follows:

$$CH_3S \xrightarrow{NO_2,O_2,HO_2,O_3,H_2O} 0.9SO_2 + 0.1H_2SO_4 \qquad \text{(R9)}$$

In addition, they assigned this a rate constant of 5.0 cm^3 $molecule^{-1}$ s^{-1} assuring

ACPD
10, 15811–15884, 2010

a near instantaneous reaction. In light of data summarized by Atkinson et al. (2004), and given the thermal instability of the CH_3SOO product, we have chosen to ignore the reaction of CH_3S with O_2 and include only reactions with O_3 and NO_2. The reaction between CH_3S and NO produces CH_3SNO, but it was not included because it photodissociates back to CH_3S+NO during the daytime resulting in a fairly short lifetime and limited presence in the atmosphere. Clearly, this is one area where future advances may require significant revision to the mechanism. The reaction with O_3 follows the net yield modeled in Zhu et al. (2006), but applies the measured rate constant in Atkinson et al. (2004).

MSO Reactions: MSO+O_3 has been observed to yield a variety of products. One, CH_2SO_2, is a relative enigma because neither NASA (1997), Finlayson-Pitts and Pitts (2000) nor Atkinson et al. (2004) provide any information on its reactivity or fate. The two remaining noteworthy reaction channels – yielding CH_3S+$2O_2$ and CH_3+SO_2+O_2 – were added to CMAQ4.6 with percent yields based on data cited by Finlayson-Pitts and Pitts (2000). Finally, MSO+NO_2 was included because it is well characterized and relatively fast.

DMSO & MSIA Reactions: Zhu et al. (2006) relied on data from Kukui et al. (2003) to model the reactions of DMSO and MSIA with OH. Their simplifications reduce a complex set of reactions into two simplified reactions that were adopted in this study (k=9.0×10^{-11} cm^3 molecule^{-1} s^{-1} for both):

$$\mathrm{DMSO + OH \rightarrow 0.9MSIA + 0.1DMSO2} \quad \text{(R10)}$$

$$\mathrm{MSIA + OH \rightarrow 0.9SO_2 + 0.1MSA} \quad \text{(R11)}$$

The net effect of the organic sulfur reaction set that starts with DMS is the production of inorganic species SO_2 and H_2SO_4, along with organic species DMSO, DMSO2, MSIA and MSA. A number of reactions involving DMS, DMSO, DMSO2 and MSIA occur in clouds.

CH_3 and CH_3O Reactions: Closure to the revised CB05 mechanism requires inclusion of reactions involving the radicals CH_3 and CH_3O. Fortunately, the chemistry of

ACPD
10, 15811–15884, 2010

these species is well characterized. CH_3 reacts fairly quickly with O and O_3 to produce HCHO or CH_3O. CH_3O reacts with O_2 to produce HCHO and HO_2, and with NO_2 to yield HCHO and HONO.

3.1.5 Comparison with other gas phase DMS mechanisms

Our comparison here with previous organic sulfur mechanisms is not meant to be a complete compilation of other work but serves as a reference point for putting this work into perspective relative to other models. Kreidenweis et al. (1991) used a photochemical model with 72 chemical reactions (and 12 photolysis reactions) to examine sulfate aerosol formation in the marine environment. However, their model contained only one reaction involving DMS oxidation by OH with SO_2 and MSA as products. This highly simplified approach was sufficient to produce a latitudinal gradient in marine sulfate similar to that reported from some measurement studies. No reactions were included that treated H_2S.

Yin et al. (1990) developed a comprehensive model of DMS and its derivatives. Their mechanism included 40 sulfur species and 140 reactions. Zaveri (1997) simplified the Yin et al. mechanism (10 organic sulfur species and 30 reactions) for use in a large-scale atmospheric model. The Zaveri model retained the major oxidation pathways from its more complex progenitor, but several reactions were combined and/or simplified to reduce computational requirements. Zaveri's work focused most attention on the fate of two radicals formed as part of the DMS-to-sulfate channels: CH_3SO_2 and CH_3SO_3. The reason for this is that CH_3SO_2 is formed as part of several reaction channels (while CH_3SO_3 is produced from some reactions involving CH_3SO_2) but its fate has been less certain than other intermediate species. The uncertainty is due to the relative importance of the thermal decomposition

$$CH_3SO_2 \rightarrow CH_3 + SO_2 \qquad \text{(R12)}$$

versus reactions of CH_3SO_2 with species such as NO_2, O_3 and HO_2. Prior to Zaveri's work, different laboratory studies of this decomposition yielded rates that differed by

ACPD
10, 15811–15884, 2010

a factor of 3×10^5. Clearly, this uncertainty – plus the uncertainty of the rate constants for chemical reactions involving CH_3SO_2 – made it difficult to know whether these reactions were of sufficient significance to include in a mechanism for marine sulfate. Zaveri concluded that the competing reactions were important and included them (plus reactions involving CH_3SO_3) in his mechanism.

The primary features of the Yin et al. mechanism, the Zaveri mechanism, and mechanisms used by Lucas and Prinn (2005) and Zhu et al. (2006), are essentially the same (although differences exist in the rate constants and branching or partitioning ratios for some of the reactions). DMS is initially attacked by OH with two reaction channels (all mechanisms), NO_3 (all mechanisms) and O (Yin et al. and Zaveri mechanisms). One DMS+OH channel produces DMSO, DMSO2, MSIA and MSA (all mechanisms, except Lucas and Prinn do not include DMSO2). The other OH channel leads to the formation of the hydroperoxy radical CH_3SCH_2OO which undergoes further reactions that produce CH_3S and, ultimately, SO_2 and H_2SO_4 (all but the Lucas and Prinn mechanism). Only the Yin et al. and Zaveri mechanisms include reactions involving CH_3SO_2 and CH_3SO_3.

The modified CB05 mechanism outlined here shares many similarities with, and borrows from, the previous work. As described earlier, both DMS+OH reaction channels, the DMS+NO_3 reaction and the DMS+O reactions are all included. We have added the DMS+Cl reaction. Rate constants have been updated using the most recent information available in the peer-reviewed literature. Our major deviation from the Yin et al. and Zaveri mechanisms is in leaving out the CH_3SO_2 and CH_3SO_3 species and their reactions. The rationale for this is as follows. The simpler Zaveri mechanism has 11 reactions with CH_3SO_2 as a product. In addition, it includes 12 reactions that involve CH_3SO_2 or CH_3SO_3 as reactants. Thus, 23 reactions are used by Zaveri (1997) to handle these two species. It is not possible to eliminate all these reactions (some are slow enough to neglect), but in all cases reactions forming CH_3SO_2 can be replaced by reactions that yield CH_3+SO_2 if we assume the thermal decomposition of CH_3SO_2 is fast in comparison with CH_3SO_2 chemical reactions.

ACPD
10, 15811–15884, 2010

A study by Kukui et al. (2000) – published after Yin et al. (1990) and Zaveri (1997), and too late to be included in the overview of Finlayson-Pitts and Pitts (2000) – examined in detail the issue of CH_3SO_2 thermal decomposition. Kukui et al. (2000) measured CH_3SO_2 behavior and their data, coupled with theory were used to develop a mathematical expression for CH_3SO_2 thermal decomposition as a function of temperature and pressure. This expression represents the CH_3SO_2 loss rate throughout the troposphere for comparison with CH_3SO_2 loss rates for its reactions with NO_2, O_3 and HO_2 at realistic concentrations based on the rate constants used by Zaveri (1997). The pressure/temperature effect on thermal decomposition was examined for a range of conditions that can occur between the ground and the top of the troposphere. Colder temperatures in the upper troposphere significantly reduce CH_3SO_2 decomposition. However, the loss rate due to decomposition in the troposphere is almost always a factor of ten or more greater than loss rates from reactions with NO_2, O_3 and HO_2. Based on this, it seems that including reactions involving CH_3SO_2 and CH_3SO_3 in a modified CB05 mechanism is likely a computational luxury that cannot be afforded at this time. Future research may further clarify the relative importance of various reaction pathways for DMS derivatives and require modifications to the approach outlined here. The current work mirrors fairly closely the mechanistic studies done previously by others.

3.2 Heterogeneous chemistry

3.2.1 Background

Modifying the gas phase chemistry in CMAQ4.6 is straightforward because the model is designed with a feature that facilitates such changes. However, the model has no such feature regarding its heterogeneous cloud chemistry module which has remained mostly unchanged from the initial version. It is based on the module used in the RADM model developed for use in acid deposition analyses conducted by the National Acid Precipitation Assessment Program of the 1980s (NAPAP, 1991). The RADM cloud chemistry module treats 5 reactions involving SO_2 oxidation by H_2O_2,

ACPD
10, 15811–15884, 2010

S(IV) ($=SO_{2\,(aq)}+HSO_3^-+SO_3^{2-}$) oxidation by O_3, HSO_3^- oxidation by peroxyacetic acid (PAA) and methylhydrogen peroxide (MHP), and S(IV) catalytic oxidation by Fe^{2+} and Mn^{2+}.

The standard CMAQ module assumes steady-state conditions within a cloud during the time integration of the kinetic equations, with gas-aqueous equilibria computed using Henry's Law constants for the following gases: SO_2, H_2SO_4, CO_2, NH_3, HNO_3, O_3, H_2CO_2 (formic acid), H_2O_2, HCl, PAA, and MHP. The dissociation of dissolved acids and bases – plus the presence of soluble salts (ammonium nitrate, sodium and potassium chloride, and magnesium and calcium carbonate) from airborne particles – contribute to an ion balance that determines droplet pH. Ion activity coefficients are computed to calculate the activities of all dissolved ionic species. The total rate of heterogeneous sulfate formation is computed as the sum of the rates of formation from the individual kinetic equations. Rate (transient) equations are integrated for 6- or 12-min periods followed by adjustments made to equilibrium concentrations of interstitial gases and aerosol species consumed or produced during the integration. The CMAQ cloud module is executed in a quasi steady-state manner with cloud chemistry pausing to allow gas chemistry to proceed before resuming the heterogeneous reactions. This method is used because it is simple to program, has low computational overhead and is easily modified. A disadvantage of this approach is that, by suspending gas phase chemistry and diffusion during integration of the heterogeneous cloud reactions, it is likely that fast-reacting species will be depleted from the gas phase within the cloud, thereby stopping some heterogeneous reactions (hence, the reason for CMAQ reducing the cloud integration time step from 12 to 6 min).

Karamchandani and Venkatram (1992) used a similar approach in their ADOM model. The ADOM heterogeneous chemical reactions are essentially the same as in RADM/CMAQ although their treatment of cloud microphysics is more sophisticated. A cloud model developed by de Valk and van der Hage (1994) for use in long range transport models also used relatively sophisticated cloud microphysics but its chemistry only treated the oxidation reactions of S(IV) by O_3 and H_2O_2. Möller and Mauers-

ACPD
10, 15811–15884, 2010

berger (1992) examined cloud chemistry from the opposite perspective, using sophisticated heterogeneous chemistry (57 aqueous reactions and equilibria) in a flow-through reactor-type model to examine the roles of various inorganic and organic reactants in sulfur oxidation and radical cycling. Their sulfur chemistry included S(IV) oxidation by O_3, H_2O_2, organic peroxides, OH, NO_3 and metal ion catalysis, but no organic sulfur reactions. In addition, they simulated the interplay between OH, H_2O_2, HO_2, O_3, NO_3 and soluble organic species in cloud droplets. Under certain conditions (especially low SO_2), clouds can be a net source of HO_2 which can be transferred into the gas phase from the droplets. At very low SO_2 (<0.1 ppbV) no net H_2O_2 destruction (because of in-cloud H_2O_2 formation) was computed, although clouds become a very effective sink for H_2O_2 when SO_2>0.5 ppbV. Möller and Mauersberger (1992) concluded that, in low SO_2 conditions, clouds play an important role in photooxidant dynamics.

Williams et al. (2002) used a one-dimensional cloud model to investigate the role of marine stratocumulus clouds as a possible source of HONO. Their calculations, based on a cloud model originated by Van den Berg et al. (2000), simulated aqueous chemistry following the CAPRAM reaction mechanism (Herrmann et al., 2000) involving 86 species and 178 reactions. Williams et al. (2002) added 26 reactions treating reactive halogen species but simplified other reactions involving peroxy radicals. Their results indicated that in-cloud HONO formation, and its effects on droplet acidity and ozone chemistry, is most likely to be important in a moderately-polluted marine environment. However, due to large uncertainties in the aqueous chemistry involved, the modest impact on photochemistry and the high computational requirements of the modified mechanism, they recommended against trying to incorporate HNO_4/HONO chemistry into larger-scale three-dimensional atmospheric chemistry models.

Global modeling of sulfate and nitrate aerosols by Park et al. (2004) using their GEOS-Chem model computed in-cloud SO_2 oxidation by O_3 and H_2O_2 and an assumed droplet pH of 4.5. They computed gas phase oxidation of DMS with yields of MSA and SO_2, but did not include DMS or MSA in the heterogeneous reactions. An aqueous chemistry model that combined oxidation of S(IV) and DMS in a relatively sim-

ACPD
10, 15811–15884, 2010

ple set of kinetic reactions was presented by Zhu (2004) and again in Zhu et al. (2006). This model included the usual reactions involving the oxidation of S(IV) species by H_2O_2 and O_3, plus reactions of DMS, DMSO, MSIA and MSA with various oxidants (O_3, OH, SO_4^-, Cl and Cl_2^-) and is based in part on new laboratory measurements of several organic sulfur species that provided a more complete kinetic mechanism for heterogeneous reactions.

Henze and Seinfeld (2006) reported major increases in secondary organic aerosol (SOA) formation from isoprene when using a parameterized aerosol formation mechanism in GEOS-Chem. Recently, Ervens et al. (2008) examined the formation of SOA by way of heterogeneous reactions involving organic compounds derived from isoprene. Two processes were modeled for producing aerosol mass from isoprene oxidation products by partitioning semivolatile organics between the gas and condensed phases using empirical partitioning ratios and modeling heterogeneous chemical reactions involving water-soluble isoprene oxidation products. The carbon aerosol yield was significant (to greater than 10 percent on the initial isoprene carbon mass in boundary layer cycling through clouds) and was dependent on the VOC/NO_x ratio. Their heterogeneous chemistry model included over 40 reactions to simulate the evolution of inorganic sulfur and organic reactants that lead to sulfate and water soluble SOA products. The release of CMAQ4.7 includes an update to the cloud chemistry that incorporates in-cloud SOA formation pathways originating with glyoxal and methylglyoxal (http://www.cmascenter.org/help/documentation.cfm?MODEL=cmaq&VERSION=4.7&temp_id=99999). Clearly, there is a need to follow up this current effort (based on version 4.6) by selectively adding organic reactions that produce SOA.

Given previous work on heterogeneous chemistry in clouds and the goal of incorporating organic sulfur reactions into CMAQ, we opted to incorporate reactions from the model of Zhu (2004) and Zhu et al. (2006) keeping many features of the old module for computational efficiency while adding new features that provide a more realistic approach to cloud chemistry. This is an incremental step in updating a model that is

ACPD
10, 15811–15884, 2010

widely used in regulatory settings and, therefore, must maintain some computational shortcuts.

3.2.2 Equilibrium species used to determine droplet acidity

Table 4 lists the gas and aerosol species used to compute droplet acidity for both the CMAQ standard and revised versions of the cloud chemistry module. The revised module adds the effects of MSIA and MSA on droplet acidity. Incorporating the reactions used by Zhu (2004) also requires the addition of Cl, Cl_2^-, SO_4^- and OH as reactants in the revised cloud module. As shown in the next section, Cl and Cl_2^- are in equilibrium with Cl^- and this relationship is included in the initial equilibrium calculation. The vapor pressure of H_2SO_4 over water is so low that it is assumed to be entirely absorbed by cloud droplets. Initial cloud droplet equilibrium concentrations are computed by calculating the Henry's Law aqueous concentrations of atmospheric gases (adjusting gas phase mixing ratios for highly soluble species), and solving a fourth-order equation in $[H^+]_{aq}$. Ion activity coefficients are subsequently calculated and ion aqueous activities are adjusted accordingly.

3.2.3 Modifications to the CMAQ set of heterogeneous reactions

The most likely source of Cl and Cl_2^- in cloud droplets is not from gas phase Cl – which is highly reactive and only expected to exist in air at extremely low concentrations – but HCl. The latter goes readily into solution where it dissociates as $HCl \rightarrow H^+ + Cl^-$. In the presence of the sulfate radical,

$$SO_4^- + Cl^- \rightarrow {SO_4}^{2-} + Cl \qquad \text{(R13)}$$

(Zhu, 2004) and $[Cl]_{aq}$ reacts with $[Cl^-]_{aq}$ to produce $[Cl_2^-]_{aq}$. Properties of SO_4^- have been measured in the laboratory (Chawla and Fessenden, 1975; Huie and Clifton, 1990), and its role in heterogeneous chemistry is described later. Also important are

ACPD
10, 15811–15884, 2010

the aqueous reactions

$$OH + Cl^- \rightarrow HOCl^- \quad \text{(R14)}$$

$$HOCl^- + H^+ \rightarrow Cl + H_2O. \quad \text{(R15)}$$

Thus, $[Cl]_{aq}$ is strongly controlled by $[SO_4^-]_{aq}$ and $[Cl^-]_{aq}$. Zhu (2004) set $[SO_4^-]_{aq}$, $[Cl]_{aq}$ and $[Cl_2^-]_{aq}$ to constant values in his model.

Reactions not included in Zhu's model (i.e., SO_2 oxidation by organic peroxides) are retained from the original CMAQ cloud chemistry module. Table 5 lists the set of all heterogeneous reactions included in the revised cloud chemistry module. Rate constants are those taken from Zhu (2004) and Zhu et al. (2006) or are currently used in CMAQ. Besides the added reactions involving MHP and PAA, the other differences between the CMAQ revisions and the Zhu's model are in the treatment of the sulfate radical, Cl and Cl^-. Zhu set $[SO_4^-]_{aq}=1\times10^{-12}$ M. This served the purposes of his test for the relative importance of various sulfur oxidation reactions. However, using a constant for aqueous SO_4^- in CMAQ could introduce an artificial source of sulfur into the model. Zhu (2004) includes reactions with SO_4^- in his study because it was found to be important during his laboratory measurements of DMSO and $CH_3SO_2^-$ oxidation. He describes three theories of the origin of SO_4^- in aqueous solution, including (1) a hypothetical reaction chain initiated by OH reacting with HSO_3^- that leads to formation of SO_5^- and eventually SO_4^-, and (2) OH reacting with HSO_4^-. The value Zhu uses for $[SO_4^-]_{aq}$ is many orders of magnitude less than the typical concentrations expected for both HSO_3^- and HSO_4^- based on reasonable atmospheric concentrations of SO_2 and H_2SO_4. A working assumption is to link $[SO_4^-]_{aq}$ to computed levels of $[HSO_3^-]_{aq}$ and $[HSO_4^-]_{aq}$ by applying a small proportionality factor to computed ion levels (based on equilibrium considerations). This is what is done in the revised CMAQ module with $[SO_4^-]=\alpha\{[HSO_3^-]+[HSO_4^-]\}$, $\alpha\leq1\times10^{-3}$.

Figure 1 illustrates the sensitivity of heterogeneous $[SO_4^{2-}]_{aq}$ formation to α and cloud droplet pH at a temperature of 298 K and pressure of 1 atm. In this example at-

ACPD
10, 15811–15884, 2010

mospheric mixing ratios were SO_2=0.4 ppbV, DMSO=DMSO2=MSIA=MSA=0.1 ppbV, O_3=30 ppbV, H_2O_2=MHP=PAA=0.1 ppbV and OH=1×10^{-10} ppbV, and cloud liquid water content (W_c) was 0.5 g m^{-3}. When pH is extremely low ($\leq$1.5), steady-state sulfate formation rates from organic and inorganic sulfur oxidation are within a factor of 10. However, the rates diverge rapidly as pH increases for all values of α so that at pH=7 sulfate formation from oxidized organic sulfur compounds exceeds that from SO_2 by 5 orders of magnitude in the absence of $[SO_4^-]_{aq}$ and much more when $[SO_4^-]_{aq}>0$. Note that, in the presence of anthropogenic sources, atmospheric levels of DMS and its oxidation products are much lower than SO_2 but this is not necessarily the case in a simulation that examines the chemistry of "natural emissions" only. In addition, droplet pH is usually <5.6 unless there is a major nearby source of alkaline emissions. Thus, for expected droplet acidities, the influence of $[SO_4^-]_{aq}$ is small when its magnitude compared to $HSO_3^-+HSO_4^-$ is one ppm or less, but its importance grows rapidly with pH and for α above 1×10^{-6}. Model sensitivity to α is explored further in Sect. 4.2

Chlorine's role in the heterogeneous chemistry of sulfate formation depends on the presence of the chloride ion. During his model testing, Zhu (2004) assumed $[Cl]_{aq}=1\times10^{-13}$ M, or a factor of 10 less than the value for $[SO_4^-]_{aq}$. In this work $[Cl]_{aq}$ is derived using Henry's Law and the gaseous mixing ratio of ambient Cl. It follows that $[Cl_2^-]_{aq}$ is then computed from $[Cl]_{aq}$ and $[Cl^-]_{aq}$ using the equilibrium relation

$$\frac{[Cl][Cl^-]}{[Cl_2^-]} = 7.14\times10^{-6}\,\mathrm{M}. \qquad \text{(R16)}$$

Of the five DMSO oxidation reactions, those involving reactions with $[Cl]_{aq}$ and $[Cl_2^-]_{aq}$ are 2 to 4 orders of magnitude slower than those in which $[OH]_{aq}$ and $[SO_4^-]_{aq}$ are reactants. Chlorine as Cl_2^- can play a larger – though not dominant – role in reactions involving $CH_3SO_2^-$. Hence, the role of chlorine in heterogeneous organic sulfur chemistry is of minor importance most of the time.

ACPD
10, 15811–15884, 2010

Of the two reactions involving DMS, the one with OH is more than a factor of 20 faster than that with O_3, but O_3 concentrations are far greater than OH making the ozone reaction the dominant pathway. For reactions with DMSO, the hierarchy of rate constants is $k_{OH} \approx k_{Cl} > k_{SO_4^-} \gg k_{Cl_2^-} \gg k_{O_3}$. Ozone is the most abundant reactant to attack DMSO by at least 2 to 3 orders of magnitude. Nevertheless, the benefit of a higher concentration is still not sufficient to make up for its lower rate constant and the OH and SO_4^- reactions will usually be the most important.

3.2.4 Generic chemical transient equation

The rate at which droplets take up gaseous pollutants can be limited by gaseous diffusion toward the droplets and by the efficiency with which molecules of certain species pass through the gas-droplet interface. These rate-limiting processes are not treated by the default CMAQ cloud chemistry module and have been added to the revised version. The following treatment is based on Seinfeld and Pandis (1998). Let the activity of water-soluble gas species i at the surface of a cloud droplet be denoted $C_{s(i)}$. Diffusion limits both outside and within the droplet and variations in chemical reaction times can result in non-uniform C_i throughout the droplet. This characteristic of reactant C_i directly affects the temporal evolution of some species and must be treated in the chemical transient equations. The rate of change of the average C_i in a droplet of radius r_d is given by

$$\frac{dC_i}{dt} = \frac{x_{mt}}{RT}\left(p_i - \frac{C_{s(i)}}{(H_A)_i}\right) + X \quad (1)$$

where x_{mt} is the mass transfer coefficient, R is the universal gas constant, T is temperature, $(H_A)_i$ is the Henry's Law constant, p_i is the atmospheric partial pressure of the species at a large distance from the droplet, and X is an aqueous chemical reaction term representing any change due to chemical reactivity. To make (1) generic we replace X with $\sum_{kj}(Q_k P_{kl}) - \sum_j (Q_i L_{ij})$ with P_{kl} representing the production rate of

ACPD
10, 15811–15884, 2010

species i from a reaction between species k and l, and L_{ij} representing the loss rate of species i through its reaction with species j. Parameter Q (defined below) is an adjustment factor to account for the non-uniformity of a species activity, C_i or C_k, within the droplet. Note that this assumes co-reactant species C_j and C_l are uniform within the drop. The transient equation then becomes

$$\frac{dC_i}{dt} = \frac{x_{\mathrm{mt}}(i)}{RT}\left(p_i - \frac{C_i}{(H_A)_i}\right) + \sum_{kl}(Q_k P_{kl}) - \sum_j (Q_i L_{ij}) \tag{2}$$

where x_{mt} is given by

$$x_{\mathrm{mt}}(i) = \left[\frac{r_{\mathrm{d}}^2 RT}{3\kappa_{\mathrm{g}}} + \frac{r_{\mathrm{d}}(2\pi M_i RT)^{1/2}}{3a_i}\right]^{-1} \tag{3}$$

with κ_{g} as the gas diffusivity, M_i the molecular weight, and a_i the accommodation coefficient. The first product term on the right hand side of (2) represents the diffusion and "sticking" tendency of species i from the air surrounding a droplet (with partial pressure difference $p_i - C_i/H_A$) to the droplet surface. The parameter a_i is the ratio of the molecules of species i that adhere to the droplet surface to the total number of molecules that impact the droplet.

In (2), Q is the ratio of the average droplet activity of the non-uniform species to its activity at the droplet surface. When Q=1 the activity (concentration) is uniform. Chemical production and loss terms are derived from the appropriate kinetic rate equations. The backward Euler implicit method is used to solve for $\frac{dC_i}{dt}$:

$$C_i^{n+1} = C_i^n + (P^{n+1} - C_i^{n+1} L^{n+1})\Delta t \tag{4}$$

(Seinfeld and Pandis, 1998). Function Q is given by

$$Q = 3\left(\frac{\coth(q)}{q} - \frac{1}{q^2}\right), \quad q = r_{\mathrm{d}}\left(\frac{kC_{\mathrm{U}}}{\kappa_{\mathrm{w}}}\right)^{1/2} \tag{5}$$

ACPD
10, 15811–15884, 2010

where k is the reaction rate constant, C_U represents the uniform species activity, and κ_w is the water diffusivity (q and Q are dimensionless). In general, $Q<1$ when $kC_U>10^8\,m^{-2}\,\kappa_w$. If $\kappa_w=1\times10^{-9}\,m^2\,s^{-1}$ ($1\times10^{-5}\,cm^2\,s^{-1}$), then the co-reactant is non-uniform when $kC_U>0.1\,s^{-1}$. This implies that the non-uniform species is consumed by chemical reaction at a rate >10 percent per second.

Unlike in the default CMAQ module, this approach requires that droplet size be defined. Cloud droplets are assumed to be monodisperse (uniform in size) to minimize computer execution time. Measured droplet size distributions described by Byers (1965) for different cloud types – ranging from fog to stratus and convectively-growing cumulus and for $0.02\,g\,m^{-3}<W_c<0.8\,g\,m^{-3}$ – were analyzed to estimate their median size characteristics. Median diameters for the analyzed droplet spectra ranged from 5 to 12 µm. Most values of W_c provided to the cloud chemistry module are in the range represented by these median diameters, but higher W_c are certainly possible. As used here, when $W_c\leq1\,g\,m^{-3}$ the cloud module calculated r_d as based on the information provided in Byers (1965). For $W_c>1$ radius was set equal to a constant ($r_d=6.15$ µm) corresponding to the maximum value derived from this empirical formula. By introducing droplet size the cloud module is enabled to accommodate size-specific droplet chemistry in the future.

3.2.5 Transient and steady-state species in cloud chemical mechanism

Unlike the original CMAQ cloud chemistry module, some chemical species other than sulfate are not assumed to be steady-state. A species is assumed to be steady-state if its droplet concentration is likely to remain nearly constant during the relatively short temporal integration of the transient equations. This is true if a species is not a reactant and is usually a good assumption for reactive species if their concentrations are controlled by a large reservoir in the gas phase (i.e., the species is only partially soluble). For example, $[SO_2]_{aq}$, $[HSO_3^-]_{aq}$ and $[SO_3^{2-}]_{aq}$ are dependent on p_{SO_2}, the partial pressure of SO_2 in air. SO_2 is moderately soluble in water so that some dissolves into

ACPD
10, 15811–15884, 2010

the aqueous phase but a considerable amount remains in the gas phase. In addition, $[HSO_3^-]_{aq}$ and $[SO_3^{2-}]_{aq}$ are partly dependent on pH which tends to vary little during the period of integration ($[H^+]_{aq}$ is treated as a steady-state species). Thus, for the short time interval when the transient equations are integrated any SO_2 and its derivative ions consumed by chemical reactions are replaced by more SO_2 from outside the cloud droplets. This allows the assumption that $[SO_2]_{aq}$, $[HSO_3^-]_{aq}$ and $[SO_3^{2-}]_{aq}$ are steady-state.

The steady-state assumption is strengthened by keeping the temporal integration interval short – currently $\leq$4 min. The original version of the CMAQ cloud module performs the temporal integration over periods of 6 to 12 min. This time period is long compared to some of the reaction rates in the module but allowed for more computational efficiency. With faster computer processors it is now feasible to shorten the integration interval. The revised module uses a minimum integration step of one minute, the exact interval depending on the consumption rate of certain key species in the reaction set. The maximum interval of four minutes also allows for more frequent updating of gas phase chemistry so that some depleted reactive species in the air are allowed to recover more quickly between cloud chemical integrations than before.

Table 6 lists all the species in the revised cloud chemistry module, indicates which are treated as steady-state, which are reactive, and which are most likely to have non-uniform droplet concentrations. There are eight species that are not steady-state and whose temporal changes are represented by transient equations. An analytical solution to this set of equations (see Appendix) is used to calculate temporal changes in cloud chemistry.

4 Behavior of the modified CMAQ model

Comparisons between the old and new cloud chemistry modules, and between different chemical pathways in the new module, provide insight into the effects of the new module on air quality simulations. All comparisons described here

ACPD
10, 15811–15884, 2010

were done using the natural emissions data set described by Smith and Mueller (2010), i.e., in the absence of anthropogenic emissions. CMAQ behavior in simulating sulfate aerosol was investigated by exercising the model in various chemical configurations to identify its sensitivity to the gas phase organic sulfur chemistry (S_{org}=DMS+DMSO+DMSO2+MSIA+MSA), cloud S_{org} chemistry, cloud cover bias, and selected cloud module parameters.

Aside from chemistry, the CMAQ configuration applied here followed that used by the VISTAS Regional Planning Organization (see http://vistas-sesarm.org/) as described in Tesche et al. (2008). The VISTAS modeling domain covers all of the continental United States, large portions of Canada, Mexico, and adjacent ocean waters. The CMAQ parent grid over this domain is 4032 km (west-east)×5328 km (north-south) and composed of 36×36 km grid cells. Meteorological fields used by CMAQ are from simulations of the MM5 meteorological model (Grell et al., 1994). Chemical boundary conditions were derived from a 2002 global simulation using the GEOS-Chem model (Jacob et al., 2005). A deviation from Tesche et al. (2008) was our use of the SMVGEAR chemical solver in place of the optimized solver available in CMAQ for use with the CBIV and CB05 mechanisms. This was necessitated by changes in the gas phase chemical reaction set that preclude use of the optimized solvers, thereby increasing substantially the execution time for the model.

4.1 Grid-averaged model time series

Time series of simulated hourly natural pollutant concentrations for 2002, when averaged over the entire modeling domain, provide insight into the joint behavior of emissions and secondary pollutants. Surface layer mixing ratios of selected gas species and aerosol concentrations were averaged for each hour and then a 24-h smoothing filter applied to suppress diurnal noise. Model output for 29 December 2001 through 10 January 2002 was dropped from the analysis due to chemical spin-up issues. The simulation ended at 00 UTC on 1 January 2003 making 31 December incomplete (based on local time). Therefore, all 2002 results are presented for 354 days. Note that all

ACPD
10, 15811–15884, 2010

time series plots include “background” contributions from pollutants advected into the domain from the boundaries.

Figure 2 plots grid-averaged surface layer annual time series of ozone, NO_y (=sum of NO, NO_2 and all other model oxidized nitrogen species) and formaldehyde (CH_2O). Both NO_y and CH_2O exhibit a clear winter minimum and summer maximum consistent with the expected seasonally-driven photochemical cycle. However, ozone is nearly constant for the first four months, declines slightly May through September, and then levels off for the remainder of the year. Simulations made by removing lightning and wildfire NO_x emissions revealed that the seasonal patterns of both sources favor higher summer ozone and in no way contribute to the observed ozone pattern (the other source of natural NO_x – soils – is too small to have a significant effect on the grid average). Thus, the winter/early spring peak in grid-average ozone is imposed on the grid from outside the modeling domain, i.e., from the boundary conditions.

The global GEOS-Chem model, the source of these boundary conditions, appears to produce a pattern of background ozone that is similar to that produced by Berntsen et al. (1999) except that their modeling also produced a summer minimum in background air arriving in the US from across the Pacific Ocean. They concluded that the higher spring ozone was attributable to Asian emissions having a greater impact at long distances in spring because of enhanced trans-Pacific transport during that time of year. Vingarzan (2004) also found a spring (May) maximum in measured background ozone at “clean” sites in Canada and the US. Finally, Oltmans et al. (2008) analyzed ozone measured at west coast sites usually uninfluenced by air from the mainland, reporting an annual pattern for 2004 that looks a lot like the ozone pattern in Fig. 2 with a March–May peak. These similarities suggest that the CMAQ grid-average seasonal ozone pattern reflects a known phenomenon.

Time series of modeled sulfur (S) species are illustrated in Fig. 3. Inorganic S (S_{inorg}=SO_2+H_2S+sulfuric acid) represents the most abundant class of gaseous sulfur compounds. Grid-average values peak above 100 pptV during several periods throughout the year. Grid-average S_{org} stays below 100 pptV, peaking in summer and falling

ACPD
10, 15811–15884, 2010

to levels well below those of S_{inorg} in winter. The S radicals (labeled "S-rad" in Fig. 3) time series is the sum of organic and inorganic gaseous S intermediate species (e.g., SH, HSO, CH_3S and CH_3SCH_2) that are very reactive, have relatively short lifetimes and represent intermediate oxidation steps between DMS and H_2S on one hand and MSIA, MSA, H_2SO_4 and sulfate on the other. S radical values peak in summer. The total gaseous S time series ("S-gas") plotted in Fig. 3 indicates that the sum of all natural gaseous species tends to remain fairly constant throughout the year with values in the 100–300 pptV range. Sulfate aerosol concentrations follow the expected seasonal cycle with grid-average values peaking near 0.3 $\mu g\,m^{-3}$ in summer.

Ammonia, NO_z ($=NO_y-NO_x$) and ammonium nitrate aerosol time series are plotted in Fig. 4. NO_z, which includes nitric acid, represents the more oxidized of the nitrogen compounds and is a better indicator than NO_x of precursors to nitrate aerosol formation. All these species follow a seasonal cycle with a grid-averaged summertime maxima. For NH_4NO_3 this represents a departure from the expectation that thermodynamics are more favorable for winter formation of the aerosol. In both winter and summer, simulated natural nitrate aerosol concentrations were primarily centered on areas with relatively high ammonia emissions. These areas were over the Pacific and Atlantic Oceans and the Gulf of Mexico, as well as in the vicinity of wildfires in the western US, Florida (winter), and eastern Canada (summer).

Secondary organic aerosols formed from precursor VOCs such as isoprene and terpene compounds, and from organic aerosol polymerization that results in non-volatile aerosols, were simulated in CMAQ4.6 using an approach developed for regional haze modeling (Morris et al., 2006) and implemented in the previous version of CMAQ. The changes introduced by Morris et al. were transferred to CMAQ4.6.

Figure 5 illustrates grid-averaged time series for all simulated natural particulate matter: sulfate, nitrate, estimated organic carbon (OC), elemental carbon (EC), fine soil dust, coarse particle mass (PM_C=particles in the 2.5–10 µm diameter range, fine sea salt and $PM_{2.5}$. All appeared consistent with expectations based on seasonal emissions behavior and the dependence of atmospheric chemistry on meteorology. Am-

ACPD
10, 15811–15884, 2010

monium sulfate/bisulfate, ammonium nitrate, and carbonaceous particles all peak in summer as does total $PM_{2.5}$ mass. Both fine dust and sea salt are highest in late winter and spring when winds are strongest. Coarse particles follow a similar pattern to that of fine dust.

Winter and summer grid-average natural ozone mixing ratios and aerosol concentrations are compared in Table 7. The difference between winter and summer "background" ozone is apparent. In the absence of anthropogenic emissions, a west-east ozone gradient is expected in winter due to the transport of anthropogenic emissions from Asia. Sulfate aerosol (including the associated ammonium component) is over a factor of two greater in summer than winter. Organic carbon aerosol mass is more than 6 times greater in summer than winter because of the combined contributions from wildfires and biogenic precursor emissions. Natural coarse particle mass is computed to be less in summer but $PM_{2.5}$ mass levels are much higher. These averages mask a great deal of spatial and temporal variability that is addressed by a future paper.

4.2 Influences of different gas and cloud chemistry treatments

Special CMAQ simulations for June 2002 investigated the influence of different gas and cloud chemistry options. June was selected because its high levels of photochemistry were expected to strongly differentiate among the different chemistry treatments. June test simulations were initiated following a common set of initial conditions derived from a preceding simulation of January–May 2002. The January–May simulation that produced the initial conditions was made using CMAQ4.6 with both revised gas and cloud chemistry options activated. Test results from the first week of June were not analyzed to allow the model to adjust to an abrupt change in internal parameters on 1 June. The various tests are summarized in Table 8. Comparisons of test results from 8–30 June are provided in the following sections.

ACPD
10, 15811–15884, 2010

4.2.1 Effect of adding reduced sulfur and chlorine gas phase chemistry: tests A and B compared

Differences between tests A and B reveal the impact of adding reduced sulfur and chlorine gas phase chemical reactions to the standard CB05 mechanism. Changes are quantified as the mean change, $\bar{\Delta}$, in variable x relative to reference variable x_0 where $\Delta = \frac{x - x_0}{x_0}$ and the average is computed at each grid cell over the time period of the test simulations. The pattern in OH showed little change during the day with more significant changes at night. The resulting average over 8–30 June (Fig. 6, top) produced decreases over land as large as 60 percent and increases over the oceans of up to 60 percent. Nighttime increases over the water are almost certainly caused by the introduction of DMS and its derivatives. These species react with many other species that also react to remove OH. Thus, S_{org} compounds act as an additional sink for species that remove OH thereby slowing the nocturnal depletion and resulting in higher nighttime levels. Widespread inland decreases in OH are the expected response to "aged S_{org}" (less DMS and more DMSO, etc.) in air advected across the continent from the west. Note that the aging of S_{org} includes formation of SO_2.

The only source of secondary sulfate aerosols in standard CMAQ4.6 is SO_2 oxidation. The relative change in SO_2 due to the change in chemistry treatment is illustrated in Fig. 6 (middle). With meteorology fixed, the SO_2 response is determined by SO_2 formation from S_{org} oxidation and to a lesser extent by changes in OH, peroxides, and ozone. Domain-wide SO_2 increases occurred because of the organic sulfur chemistry added to the model. The largest increases – often 3 orders of magnitude and more – occurred over and downwind of grid cells experiencing the highest emission rates of DMS and H_2S.However, these dramatic increases are due in large part because many of the most affected grid cells have little or no SO_2 emissions.

Aerosol sulfate is enhanced everywhere by the chemistry changes (Fig. 6, bottom) but the greatest increases occurred near sources of DMS and H_2S. Over many cells the increases exceeded a factor of 10. For ocean cells sulfate averages increased by

ACPD
10, 15811–15884, 2010

nearly 2 μg m^{-3} in some places. Inland sulfate increases averaged 0.1–0.2 μg m^{-3} over south Texas and Florida with smaller increases elsewhere.

4.2.2 Effect of adding organic sulfur cloud chemistry: tests B and C compared

Test C replaced the default CMAQ cloud chemistry module with one that included S_{org} reactions. The OH radical responded with mostly small increases over most of the domain (Fig. 7, top). Overall, changes in OH were far smaller than those attributable to the change in gas phase chemistry and were generally in response to the consumption of S_{org} by the heterogeneous reactions. Changes in SO_2 (Fig. 7, middle) were negative over most of the domain. The SO_2 response to cloud chemistry changes is caused partly by moving S_{org} from the gas phase, where it oxidizes to SO_2, to the aqueous phase in which SO_2 does not form. However, changes in the timing between cloud chemistry integration and the gas-phase chemistry may also play a role (see Sect. 4.2.3).

Changes in aerosol sulfate in response to cloud chemistry changes (Fig. 7, bottom) occurred primarily where clouds were most prevalent. Significant reductions in sulfate from reduced SO_2 gas phase oxidation were offset by enhanced sulfate formation in clouds. Widespread sulfate increases occurred over the Gulf of Mexico, Florida and the western Atlantic east of Florida where diagnostics indicate a persistent cloud cover for the month. Generally, the cloud chemistry changes resulted in higher sulfate across the eastern half of the US. Sulfate increased over the Pacific Ocean off the North American coast by an average of 0.05–0.1 μg m^{-3} due to cloud chemistry but inland cloud effects were much smaller.

4.2.3 Effect of cloud OH uptake: tests D and B compared

Test D was done to determine the relative influence of the S_{org} versus SO_2 cloud chemistry as well as the differences between the old and new cloud module SO_2 chemistry. The former comparison, enabled by not allowing OH to enter the clouds, was facili-

ACPD
10, 15811–15884, 2010

tated because aqueous OH reactions involving S_{org} are the dominant reactions in the clouds (reactions involving the sulfate radical and chlorine species were of much less significance because of the low value for α – see later comparison of tests E and F). With both tests B and D using the modified gas phase chemical mechanism, their differences illustrate how the original and modified SO_2 cloud chemistry differentially influence sulfate formation.

Differences in air concentrations of SO_2 and sulfate were generally small across the model domain. This is partly because cloudy cells accounted for only 5 percent of all grid cells. However, even in cells that experienced significant cloud cover, f_{cc}, (i.e., whenever f_{cc}>10 percent for a given hour) the differences in hourly averaged SO_2 and sulfate were usually small. Surface SO_2 mixing ratios beneath cloudy cell columns with f_{cc}>0.1 had a tendency to have somewhat higher values in test D compared to test B but the result is misleading. More cells experienced higher SO_2 in test D but the differences were generally <20 percent and were associated with those cells experiencing mixing ratios <1 ppbV. SO_2 decreases were larger – some exceeding 75 percent – but those tended to occur in the cells with mixing ratios >1 ppbV. The net effect was for higher SO_2 in test D with the domain-averaged value (under clouds) increasing from 0.02 ppbV to 0.23 ppbV. Sulfate also responded in test D with higher values under clouds. The pattern in sulfate differences as seen in Fig. 8 mimicked that in SO_2 with small increases occurring in cells with low sulfate and larger decreases occurring in cells with higher sulfate. The net result across the domain was for an increase in sulfate under cloudy conditions from 0.01 to 0.29 $\mu g\, m^{-3}$. The effect on all cells was far smaller, however, due to the low spatial coverage of simulated clouds.

The different results between tests D and B are associated with differences in the behavior of the original and modified cloud chemistry modules in their treatment of SO_2 chemistry (although some minor differences are caused by the reactions of S_{org} as previously mentioned). The revised cloud module slows down SO_2 reactions by putting rate limits on droplet uptake of gaseous reactants and by computing average droplet concentrations (for fast-reacting species like H_2O_2) that are below the idealized

ACPD
10, 15811–15884, 2010

concentrations computed in the original cloud module. However, the effect of shortening the integration time step for droplet chemistry from 6–12 min down to 1–4 min can have an additional effect of increasing sulfate production under certain conditions (e.g., when reactants would otherwise be depleted for longer time steps) by allowing the gas chemistry to better keep pace with the droplet chemistry. The net effect as illustrated in Fig. 8 appears to be sulfate concentration differences that depend on which cloud module characteristic is more important for a particular situation. Note that comparisons of test results showed that the changes to SO_2 and sulfate concentrations were not caused by differences in calculated wet deposition scavenging.

4.2.4 Effect of enhancing cloud cover: tests E and C compared

There is evidence that cloud cover is underestimated in CMAQ. This issue has been addressed before (Mueller et al., 2006). For the current modeling, total sky cloud cover was examined using observations from 7 surface stations across the US[1] and three in the Bahamas.[2] Data were compared with CMAQ output. This allows for a test of how well CMAQ replicates cloud cover by combining cloud output from MM5 with its own sub-grid scale diagnostic cloud module. The comparison suffers from imperfect observations (they are all automated and do not include clouds above 3700 m) but is believed to be at least as representative of model performance as would be a comparison based on satellite imagery (the latter suffers from an inability to detect lower clouds beneath elevated cloud cover). CMAQ underestimated cloud cover for 2002 at all 7 US stations, with "clear" (<1/8 cover) being the predominant condition in the model for all but Tampa, Florida. However, for the Bahamian stations the model actually overestimated cloud cover. This appears symptomatic of a CMAQ diagnostic issue over warm waters, including the Gulf of Mexico, where persistent cloud cover was a characteristic problem.

[1] Los Angeles, Denver, Houston, Atlanta, Tampa, Chicago and Boston.

[2] Freeport, George Town and Nassau.

ACPD
10, 15811–15884, 2010

A low cloud cover bias across most of the CMAQ domain suggests that the role of clouds in S_{org} and SO_2 oxidation may be underestimated. This may potentially underestimate natural sulfate aerosol levels. Test E examined the potential impact of this problem on sulfate by simulating enhanced cloud cover over Pacific Ocean grid cells. This was done by inserting clouds into model layers between 250 and 750 m above sea level when clouds were absent. In addition, minimum cloud liquid water content was arbitrarily set to 0.5 g m^{-3}, a value that is roughly half of the highest values used in CMAQ (and output from MM5). This ensured that clouds were able to process air at lower levels moving into the domain from the west throughout the period. Differences between test E and test C were used to estimate the upper limit to model sensitivity to clouds. Unlike previous tests, the effect on OH was fairly small ($-0.1 \leq \bar{\Delta}_{OH} \leq 0.05$)with most changes being negative over the Pacific Ocean.

Responses of SO_2 and aerosol sulfate are plotted in Fig. 9. Decreases in SO_2 in response to increased cloud cover (Fig. 9, top) occurred over the Pacific Ocean, mostly in the range of −40 to −80 percent. Inland over the continent – and downwind from the artificially enhanced cloud cover – SO_2 changes were ±20 percent and generally decreased as expected from west to east. Sulfate changes (Fig. 9, bottom) were likewise positive over the Pacific Ocean and decreased going eastward. Most ocean grid cells had increases of 20–30 percent but some isolated areas experienced increases in excess of 10^4. These latter cells were those that had extremely low sulfate values in the reference simulation and the large relative changes did not indicate a problem with excessively high values. Absolute sulfate changes were no more than 0.15 µg m^{-3} in cells experiencing the highest relative sulfate increases, and the highest simulated concentrations over water were about 2 µg m^{-3}.

4.2.5 Model sensitivity to the aqueous sulfate radical: tests F and C compared

The aqueous sulfate radical, SO_4^-, is an integral part of the revised cloud chemistry model as implemented from Zhu (2004). The parameter α used in the revised CMAQ cloud module determines the magnitude of $[SO_4^-]_{aq}$ that reacts with $DMSO_{aq}$ and

ACPD
10, 15811–15884, 2010

$MSIA_{aq}$ (as dissociated to $[CH_3SO_2^-]_{aq}$). Zhu (2004) set $[SO_4^-]_{aq}=1\times10^{-12}$ M. His modeling used an atmospheric SO_2 mixing ratio at cloud height of about 6 pptV (CMAQ values for June were ≤20 pptV over the Pacific) and he assumed a cloud droplet pH of 5. Using published Henry's Law and dissociation constants for SO_2 yields $[HSO_3^-]_{aq}=1\times10^{-8}$ M at 298 K near sea level. This is equivalent to $\alpha=1\times10^{-4}$ in the absence of sulfuric acid. The rate constants for reactions involving the sulfate radical made it the second most important reactant in his model after OH (Zhu, 2004). Based on this, we conservatively assumed $\alpha=1\times10^{-6}$ for all but test F thereby maximizing the contribution from OH relative to SO_4^-. However, at a realistic cloud droplet pH of 4 the value of α would be 1×10^{-3} and the sulfate radical would make a much larger contribution to the cloud S_{org} chemistry, rivaling OH as the primary reactant oxidizing DMSO. We tested the sensitivity of CMAQ to α by increasing it to 1×10^{-3}. Thus, test F results represent an upper limit to the model's sensitivity to sulfate radical in-cloud reactions.

Figure 10 illustrates the relative sensitivity of SO_2 and sulfate to α. The average change $\bar{\Delta}_{SO_2}$ (Fig. 10, top) produced by increasing α was a net SO_2 reduction over the model domain of only 2.4 percent. However, SO_2 reductions averaged >5 percent over the Pacific Ocean where S_{org} was more prevalent. In Fig. 10 (bottom) $\bar{\Delta}_{SO_4}$ is seen to be positive across the domain (+5 percent) but especially over the Gulf of Mexico and southeastern US (+26 percent). The relative increase in sulfate is larger where sulfate concentrations are originally smaller and where more persistent cloud cover has a greater influence on sulfate formation. We conclude that modeled sulfate sensitivity to α is small on average but can be significant in regions with persistent cloud cover. Note that the relatively large change over the southeastern US and adjacent ocean is only about 0.035 μg m^{-3} in absolute terms.

ACPD
10, 15811–15884, 2010

4.2.6 Ozone and OC sensitivity to different CMAQ chemistry configurations

The influence of different CMAQ chemistry configurations on ozone was also examined. The case can be made that model O_3 results from tests B, C and D were very similar to each other and were significantly different from test A. Test A (original model) produced higher O_3 across most of the grid for most hours with a grid-average difference of about 3.5 ppbV compared to test B in which the gas-phase chemistry was modified to include chlorine, S_{org} and H_2S reactions. This difference is likely due mainly to the extra sink for various radicals included in the gas chemistry for S_{org} and H_2S. Test C (implementation of revised cloud model with S_{org} chemistry) produced on average 1.5 ppbV more O_3 than test B. Blocking OH uptake in clouds in test D resulted in an average reduction in O_3 (from test C) of only 0.25 ppbV.

Differences in OC between tests A and C were also minor. This is primarily because organic aerosol mass is dominated by wildfire emissions that are unaffected by the model chemical schemes. However, SOA is somewhat sensitive to the model chemistry because of the role played by OH in oxidizing VOCs. Thus, in areas where total organic aerosol mass is primarily composed of SOA mass, the influence of chemical schemes may be important. Average relative differences in SOA (and OC) for tests A and C were nearly nonexistent over the Pacific Ocean but this is not surprising given the nearly total absence of precursor VOC species there. The largest differences occurred over the Gulf of Mexico with decreases averaging about 7 percent (Atlantic Ocean decreases were only about 2–3 percent). SOA decreases were driven by OH consumption by S_{org} both in the gas and aqueous phases. Inland, the largest SOA effects occurred over the Southeast US with SOA decreases averaging nearly 5 percent. Across the northern US and Canada SOA increases averaging about 3–4 percent were modeled, perhaps due to transport from the south of more unreacted VOCs. Thus, the introduction of S_{org} chemistry has a small negative impact on SOA – and total OC – mass over the Atlantic Ocean/Gulf of Mexico and adjacent inland areas, and a compensating effect farther north.

ACPD
10, 15811–15884, 2010

In certain grid cells influenced by wildfire emissions, hourly OC differences as large as $\pm 400\,\mu g\,m^{-3}$ or more occurred during the 8–30 June test A overlap with test C. Typically, offsetting differences of opposite sign and nearly equal magnitude occurred in adjacent grid cells. The mechanism for this effect is not clear but could be associated with the interaction of S_{org} with OH. In any event, the net effect when averaged over several hours and across large regions was miniscule.

4.3 Simulated concentrations in the marine boundary layer

Table 9 compares average simulated S_{org}, SO_2 and sulfate concentrations in the Pacific Ocean marine boundary layer with average values measured globally by various researchers. The observations represent a variety of measurement techniques, locations and seasons. Reported values were averaged for comparison with the CMAQ June 2002 results from test C (revised model). Simulated DMS values are consistent with and slightly lower than those reported from field data, the latter usually based on summer season measurement campaigns. Simulated DMSO, MSA and SO_2 levels are also lower than the mean observations. This implies that the test C model configuration may underestimate DMS oxidation rates and, thus, oxidation products. The exception is sulfate with model values being somewhat higher than those measured by several investigators.

A second comparison was made (Table 9) with observations using model results from test F in which DMS oxidation and sulfate formation were maximized by increasing the role of the sulfate radical in cloud oxidation of DMSO. As expected, this reduced DMS concentrations about 10 percent, and decreased DMSO by nearly 50 percent. It also increased MSA by 50–60 percent. However, S_{org} oxidation product SO_2 decreased about 5 percent and average sulfate aerosol increased slightly. It is possible that, in test F over the Pacific Ocean, enhanced cloud oxidation of S_{org} was mostly offset by lower gas-phase oxidation leading to little net change in SO_2 and only a small increase in sulfate.

ACPD
10, 15811–15884, 2010

Another way to examine these data is to normalize DMSO, MSA, SO_2 and sulfate by DMS concentrations to determine how closely the relative abundance of simulated DMS oxidation products mimic the observed relative levels thereby providing a better way to evaluate the model's S_{org} chemistry. Using results from tests C and F, CMAQ values of DMSO/DMS over the Pacific Ocean were 0.005–0.008 compared to an observed ratio of about 0.01. Likewise, normalized MSA in CMAQ was 0.030–0.067 compared to observe values of 0.067–0.560, and normalized CMAQ SO_2 was 0.076–0.080 compared with ∼0.40 observed. Finally, normalized sulfate from CMAQ was 0.31–0.46 compared with 0.23–1.60 observed. The only simulated species whose normalized concentrations were clearly not consistent with observed normalized values was SO_2. However, observed maritime SO_2 is represented here by data from only one study which may not be representative of the larger population of actual conditions.

These results suggest that the revised CMAQ model chemistry, acting on the new ocean emissions of DMS, does a reasonable job simulating the behavior of organic sulfur. Intermediate products DMSO, MSA and SO_2 (and, by implication, DMSO2 and MSIA) tend to fall on the low side of observed values when normalized by DMS. Simulated sulfate levels seem to be relatively unbiased compared to observations made over the oceans.

5 Summary

A revised cloud chemistry module and modifications to the CMAQ4.6 CB05 gas phase chemical mechanism have been tested as a prelude to detailed modeling of natural air pollutant levels. This model, coupled with a natural emissions data base, provides a means of exploring contributions from natural systems/processes to total air quality over the US. Simulated natural+background ozone across the modeling domain has a winter-spring maximum consistent with observations at background sites along the western edge of North America. Various aerosol components have either summer or winter-spring maxima depending on their means of formation.

ACPD
10, 15811–15884, 2010

The most notable effects of introducing gas-phase and cloud S_{org} and gas-phase H_2S chemistry changes in CMAQ4.6 are:

- Slight overall decreases in natural ozone – averaging 2 ppbV in summer – and attributable to decreases in OH and other oxidant radicals.
- Sulfate increases of up to 2 $\mu g\,m^{-3}$ on an hourly basis were found over the Pacific Ocean in areas far removed from SO_2 sources, and increases of nearly 1 $\mu g\,m^{-3}$ occurred over the Gulf of Mexico. The largest inland increases occurred over the Southeast US along coastal areas. In the vicinity of high SO_2 emissions (e.g., wildfires), the revised chemistry occasionally reduced sulfate levels, sometimes considerably.
- One hour changes in natural organic aerosol mass in response to the added sulfur chemistry were generally moderate except in the vicinity of wildfires where variations of ± several hundred $\mu g\,m^{-3}$ sometimes occurred during a few hours. However, across the domain, natural organic aerosol mass changes averaged $<\pm 0.1\,\mu g\,m^{-3}$ in June.
- In locations over the Pacific Ocean where continuous cloud cover was added to test model sensitivity to cloud presence, modeled sulfate concentrations at the surface increased as much as 0.15 $\mu g\,m^{-3}$ and total sulfate concentrations of up to 2 $\mu g\,m^{-3}$ occurred. Modeled sulfate sensitivity to the aqueous sulfate radical was smaller, with sulfate increasing by 26 percent over the Gulf of Mexico but totaling $<0.04\,\mu g\,m^{-3}$ at most.
- Simulated levels of DMS are realistic compared with observations for similar marine environments. Modeled levels of DMS oxidation products (DMSO, MSA and SO_2) are generally lower, on average, than observations but DMSO and MSA concentrations normalized by DMS are on the lower end of the range in observed normalized values. Sulfate responded positively to increased cloud cover and in-

ACPD
10, 15811–15884, 2010

clouds levels of the sulfate radical, and simulated sulfate concentrations over the Pacific Ocean were similar to those reported by field measurements

As for the sulfate radical scaling factor α, model results for sulfate do not appear to be very sensitive overall to its magnitude between 1×10^{-6} and 1×10^{-3} although the model response could be greater when the model is run with a combined natural and anthropogenic emissions data set. The importance of α depends on the presence of substantial cloud cover. A scaling factor toward the upper end of this range, given the tendency for the model to underestimate DMS oxidation products, may produce more realistic effects from the sulfate radical but its importance will depend on the availability of SO_2. The effects of the sulfate radical will be most important in coastal areas where DMS oxidation products are most abundant.

One potential consequence of the revised set of chemical reactions, requiring further testing to verify, is the decrease in $SO_2 \rightarrow$ sulfate oxidation efficiency in some anthropogenic SO_2 plumes when the enhanced natural emissions and "standard" anthropogenic emissions inventories are combined. This effect was seen in natural SO_2 plumes from wildfires and is likely associated with the increased competition for OH cited above. The revised model (with implementation of an updated SOA formation scheme) described here represents a new tool for air quality management because it provides a means of evaluating more realistically the influence of natural trace gas emissions on total air pollutant levels.

Appendix A

Analytical solution to the heterogeneous chemical transient equations

The equations in this appendix use subscripts to denote the various chemical species. Table A1 is a key that defines the subscript values in terms of the species they represent. The set of heterogeneous chemical transient equations in the modified CMAQ4.6 cloud chemistry module consists of the following:

ACPD
10, 15811–15884, 2010

Sulfate:

$$\frac{dC_4}{dt} = \frac{1}{\gamma_2}\left[\begin{array}{l}\gamma_1 k_{21,23} Q_{21(23)} \bar{C}_{23} C_{21} + 0.7 k_{22,31} \bar{C}_{31} C_{22} + \gamma_1^2 k_{16,23} \bar{C}_{23} C_{16} \\ +\gamma_1 k_{17,31} \bar{C}_{31} C_{17} + \gamma_1 k_{5,7} Q_{7(5)} \bar{C}_5 C_7 + (k_{1,24} \bar{C}_1 \bar{C}_{24} + \gamma_1 k_{5,24} \bar{C}_5 \bar{C}_{24} \\ +\gamma_2 k_{6,24} \bar{C}_6 \bar{C}_{24} + \gamma_1 k_{5,25} Q_{25(5)} \bar{C}_5 \bar{C}_{25} + \gamma_1 k_{5,26} \bar{C}_5 \bar{C}_{26})\end{array}\right] \quad \text{(A1)}$$

H_2O_2:

$$\frac{dC_7}{dt} = g(7,T)\left[p_7 - \frac{C_7}{(H_A)_7}\right] - \gamma_1 k_{5,7} Q_{7(5)} \bar{C}_5 C_7 \quad \text{(A2)}$$

$CH_3SO_2^-$:

$$\begin{aligned}\frac{dC_{16}}{dt} &= \left(k_{21,23} Q_{21(23)} \bar{C}_{23} + k_{21,32} Q_{21(32)} \bar{C}_{32} + k_{21,33} \bar{C}_{33}\right) C_{21} \\ &\quad - \left(k_{16,31} \bar{C}_{31} + k_{16,23} \bar{C}_{23} + k_{16,33} \bar{C}_{33}\right) C_{16}\end{aligned} \quad \text{(A3)}$$

$CH_3SO_3^-$:

$$\frac{dC_{17}}{dt} = \left(k_{16,31} \bar{C}_{31} + k_{16,23} \bar{C}_{23} + k_{16,33} \bar{C}_{33}\right) C_{16} - k_{17,31} \bar{C}_{31} C_{17} \quad \text{(A4)}$$

MSIA:

$$\frac{dC_{18}}{dt} = g(18,T)\left[p_{18} - \frac{C_{18}}{(H_A)_{18}}\right] C_{18} + k_{21,31} Q_{21(31)} \bar{C}_{31} C_{21} + \frac{\bar{C}_{11}}{k_{18}} \frac{dC_{16}}{dt} \quad \text{(A5)}$$

MSA:

$$\frac{dC_{19}}{dt} = g(19,T)\left[p_{19} - \frac{C_{19}}{(H_A)_{19}}\right] C_{19} + 0.3 k_{22,31} \bar{C}_{31} C_{22} + \frac{\bar{C}_{11}}{k_{19}} \frac{dC_{17}}{dt} \quad \text{(A6)}$$

DMSO:

$$\begin{aligned}\frac{dC_{21}}{dt} &= g(21,T)\left[p_{21} - \frac{C_{21}}{(H_A)_{21}}\right] + k_{20,24} Q_{20,24} \bar{C}_{20} \bar{C}_{24} + k_{20,31} Q_{20(31)} \bar{C}_{20} \bar{C}_{31} \\ &\quad - k_{21,24} C_{21} \bar{C}_{24} - k_{21,31} Q_{21(31)} C_{21} \bar{C}_{31} - k_{21,23} Q_{21(23)} C_{21} \bar{C}_{23} \\ &\quad - k_{21,32} Q_{21(32)} C_{21} \bar{C}_{32} - k_{21,33} C_{21} \bar{C}_{33}\end{aligned} \quad \text{(A7)}$$

ACPD
10, 15811–15884, 2010

DMSO2:

$$\frac{dC_{22}}{dt} = g(22,T)\left[p_{22} - \frac{C_{22}}{(H_A)_{22}}\right] + k_{21,24}\bar{C}_{24}C_{21} - k_{22,31}\bar{C}_{31}C_{22} \quad \text{(A8)}$$

where individual variables (activities) are denoted by C_j with subscript j indicating the species index number (Table A1). γ_1 and γ_2 are ion activity coefficients. Parameters k, Q, $\bar{C}$, g, p, and H_A with subscripts omitted are all known constants at temperature T and are defined as follows:

k_{ij}: rate constant for reaction between species i and j

$Q_{i(j)}$: concentration adjustment coefficient for non-uniform species i reacting with uniform species j ($Q_{20,24}$ is an exception; see below).

$Q_{20,24}$: Both species 20 and 24 May be non-uniform and this quantity must be computed following (5) in the main text, $Q_{20,24} = f(q), q = r_d\left(\frac{k_{20,04}\max(C_{20},C_{24})}{\kappa_w}\right)^{1/2}$

$\bar{C}_i$: activity of steady-state species i (=concentration for non-ionic species)

$g(i,T)$: mass transfer function for gas species i at temperature T; [representing $\frac{x_{\mathrm{mt}(i)}}{RT}$ (see paper Eq. 3)]

p_i: gas partial pressure of species i

$H_{A(i)}$: Henry's Law constant for species i

Equations (A1) through (A8) are linear. Their solutions can be obtained by integrating these equations with time. Since the solutions of some equations are dependent on those of others, the procedure for solving equations (A1) through (A8) is given in this order: C_{21}, C_{22}, C_{16}, C_{17}, C_7, C_{18}, C_{19}, and C_4. The initial conditions are $C_i(t=0)=B_i$, where i=21,22,16,17,7,18,19, and 4.

Integrating (A7) with time after proper manipulation and simplification leads to

$$C_{21}(t) = \frac{\beta_{21}B_{21} - \alpha_{21}}{\beta_{21}}e^{-\beta_{21}t} + \frac{\alpha_{21}}{\beta_{21}}, \quad \text{(A9)}$$

with coefficients

$$\alpha_{21} = g(21,T)p_{21} + k_{20,24}Q_{20,24}\bar{C}_{20}\bar{C}_{24} + k_{20,31}Q_{20(31)}\bar{C}_{20}\bar{C}_{31}, \quad \text{(A10)}$$

ACPD
10, 15811–15884, 2010

$$\beta_{21} = \frac{g(21,T)}{(H_A)_{21}} + k_{21,24}\bar{C}_{24} + k_{21,31}Q_{21(31)}\bar{C}_{31} + k_{21,23}Q_{21(23)}\bar{C}_{23} + k_{21,32}Q_{21(32)}\bar{C}_{32} + k_{21,33}\bar{C}_{33}. \quad \text{(A11)}$$

Similarly, the solution for (A8) after substituting C_{21} with (A9) is given by

$$C_{22}(t) = \frac{\eta_{22}}{\beta_{22}-\beta_{21}}e^{-\beta_{21}t} + \left(B_{22} - \frac{\eta_{22}}{\beta_{22}-\beta_{21}} - \frac{\alpha_{22}}{\beta_{22}}\right)e^{-\beta_{22}t} + \frac{\alpha_{22}}{\beta_{22}}, \quad \text{(A12)}$$

where

$$\begin{cases} \alpha_{22} = g(22,T)p_{22} + \frac{\alpha_{21}}{\beta_{21}}k_{21,24}\bar{C}_{24}, \\ \beta_{22} = \frac{g(22,T)}{(H_A)_{22}} + k_{22,31}\bar{C}_{31}, \\ \eta_{22} = k_{21,24}\bar{C}_{24}\frac{\beta_{21}B_{21}-\alpha_{21}}{\beta_{21}}. \end{cases} \quad \text{(A13)}$$

Substituting (A9) into (A3) and integrating with time results in

$$C_{16}(t) = \frac{\eta_{16}}{\beta_{16}-\beta_{21}}e^{-\beta_{21}t} + \left(B_{16} - \frac{\eta_{16}}{\beta_{16}-\beta_{21}} - \frac{\alpha_{16}}{\beta_{16}}\right)e^{-\beta_{16}t} + \frac{\alpha_{16}}{\beta_{16}}, \quad \text{(A14)}$$

where

$$\begin{cases} \alpha_{16} = \frac{\alpha_{21}}{\beta_{21}}\left(k_{21,23}Q_{21(23)}\bar{C}_{23} + k_{21,32}Q_{21(32)}\bar{C}_{32} + k_{21,33}\bar{C}_{33}\right), \\ \beta_{16} = k_{16,31}\bar{C}_{31} + k_{16,23}\bar{C}_{23} + k_{16,33}\bar{C}_{33}, \\ \eta_{16} = \frac{\alpha_{16}}{\alpha_{21}}(\beta_{21}B_{21} - \alpha_{21}). \end{cases} \quad \text{(A15)}$$

Substituting (A14) into (A4) and integrating with time yields

$$C_{17}(t) = \frac{\eta_{17}}{\beta_{17}-\beta_{21}}e^{-\beta_{21}t} + \left(B_{17} - \frac{\eta_{17}}{\beta_{17}-\beta_{21}} - \frac{\delta_{17}}{\beta_{17}-\beta_{16}} - \frac{\alpha_{17}}{\beta_{17}}\right)e^{-\beta_{17}t} + \frac{\delta_{17}}{\beta_{17}-\beta_{16}}e^{-\beta_{16}t} + \frac{\alpha_{17}}{\beta_{17}} \quad \text{(A16)}$$

ACPD
10, 15811–15884, 2010

where

$$\begin{cases} \alpha_{17} = \frac{\alpha_{16}}{\beta_{16}}\left(k_{16,31}\bar{C}_{31} + k_{16,23}\bar{C}_{23} + k_{16,33}\bar{C}_{33}\right), \\ \beta_{17} = k_{17,31}\bar{C}_{31}, \\ \eta_{17} = \frac{\eta_{16}}{\beta_{16}-\beta_{21}}\left(k_{16,31}\bar{C}_{31} + k_{16,23}\bar{C}_{23} + k_{16,33}\bar{C}_{33}\right), \\ \delta_{17} = \left(B_{16} - \frac{\eta_{16}}{\beta_{16}-\beta_{21}} - \frac{\alpha_{16}}{\beta_{16}}\right)\left(k_{16,31}\bar{C}_{31} + k_{16,23}\bar{C}_{23} + k_{16,33}\bar{C}_{33}\right). \end{cases} \quad \text{(A17)}$$

Next, integrating (A2) gives

$$C_7(t) = \frac{\beta_7 B_7 - \alpha_7}{\beta_7} e^{-\beta_7 t} + \frac{\alpha_7}{\beta_7} \quad \text{(A18)}$$

where

$$\alpha_7 = g(7,T)p_7, \quad \text{(A19)}$$

$$\beta_7 = \frac{g(7,T)}{(H_A)_7} + \gamma_1 k_{5,7} Q_{7(5)} \bar{C}_5. \quad \text{(A20)}$$

Substituting (A9) and (A14) into (A5) and integrating with time leads to

$$C_{18}(t) = \frac{\delta_{18}}{\beta_{18}-\beta_{16}} e^{-\beta_{16} t} + \left(B_{18} - \frac{\eta_{18}}{\beta_{18}-\beta_{21}} - \frac{\delta_{18}}{\beta_{18}-\beta_{16}} - \frac{\alpha_{18}}{\beta_{18}}\right) e^{-\beta_{18} t} + \frac{\eta_{18}}{\beta_{18}-\beta_{21}} e^{-\beta_{21} t} + \frac{\alpha_{18}}{\beta_{18}}, \quad \text{(A21)}$$

where

$$\begin{cases} \alpha_{18} = g(18,T)p_{18} + \frac{\alpha_{21}}{\beta_{21}} k_{21,31} Q_{21(31)} \bar{C}_{31}, \\ \beta_{18} = \frac{g(18,T)}{(H_A)_{18}}, \\ \eta_{18} = k_{21,31} Q_{21(31)} \bar{C}_{31} \frac{(\beta_{21} B_{21} - \alpha_{21})}{\beta_{21}} - \frac{\bar{C}_{11}}{k_{18}} \frac{\beta_{21}\eta_{16}}{(\beta_{16}-\beta_{21})}, \\ \delta_{18} = -\frac{\beta_{16}\overline{C_{11}}}{k_{18}}\left(B_{16} - \frac{\eta_{16}}{\beta_{16}-\beta_{21}} - \frac{\alpha_{16}}{\beta_{16}}\right). \end{cases} \quad \text{(A22)}$$

ACPD
10, 15811–15884, 2010

Next, substituting (A12) and (A16) into (A6) and integrating with time results in

$$C_{19}(t) = \frac{\theta_{19}}{\beta_{19}-\beta_{16}}e^{-\beta_{16}t} + \frac{\lambda_{19}}{\beta_{19}-\beta_{17}}e^{-\beta_{17}t} + \frac{\delta_{19}}{\beta_{19}-\beta_{21}}e^{-\beta_{21}t} + \frac{\eta_{19}}{\beta_{19}-\beta_{22}}e^{-\beta_{22}t} + \left(B_{19} - \frac{\eta_{19}}{\beta_{19}-\beta_{22}} - \frac{\delta_{19}}{\beta_{19}-\beta_{21}} - \frac{\lambda_{19}}{\beta_{19}-\beta_{17}} - \frac{\theta_{19}}{\beta_{19}-\beta_{16}} - \frac{\alpha_{19}}{\beta_{19}}\right)e^{-\beta_{19}t} + \frac{\alpha_{19}}{\beta_{19}}, \quad \text{(A23)}$$

where

$$\begin{cases} \alpha_{19} = g(19,T)p_{19} + 0.3k_{22,31}\bar{C}_{31}\frac{\alpha_{22}}{\beta_{22}}, \\ \beta_{19} = \frac{g(19,T)}{(H_A)_{19}}, \\ \eta_{19} = 0.3k_{22,31}\bar{C}_{31}\left(B_{22} - \frac{\eta_{22}}{\beta_{22}-\beta_{21}} - \frac{\alpha_{22}}{\beta_{22}}\right), \\ \delta_{19} = 0.3k_{22,31}\bar{C}_{31}\cdot\frac{\eta_{22}}{\beta_{22}-\beta_{21}} - \frac{\bar{C}_{11}}{k_{19}}\cdot\frac{\beta_{21}\eta_{17}}{(\beta_{17}-\beta_{21})}, \\ \lambda_{19} = -\frac{\beta_{17}\bar{C}_{11}}{k_{19}}\left(B_{17} - \frac{\eta_{17}}{\beta_{17}-\beta_{21}} - \frac{\delta_{17}}{\beta_{17}-\beta_{16}} - \frac{\alpha_{17}}{\beta_{17}}\right), \\ \theta_{19} = -\frac{\bar{C}_{11}}{k_{19}}\cdot\frac{\beta_{16}\delta_{17}}{(\beta_{17}-\beta_{16})}. \end{cases} \quad \text{(A24)}$$

Finally, integrating equation (A1) with time and substituting (A9), (A12), (A14), (A16), and (A18) for C_{21}, C_{22}, C_{16}, C_{17}, and C_7, we obtain

$$C_4(t) = \alpha_4 t - \frac{\beta_4}{\beta_{21}}e^{-\beta_{21}t} - \frac{\eta_4}{\beta_7}e^{-\beta_7 t} - \frac{\delta_4}{\beta_{22}}e^{-\beta_{22}t} - \frac{\lambda_4}{\beta_{16}}e^{-\beta_{16}t} - \frac{\theta_4}{\beta_{17}}e^{-\beta_{17}t} + \left(B_4 + \frac{\beta_4}{\beta_{21}} + \frac{\eta_4}{\beta_7} + \frac{\delta_4}{\beta_{22}} + \frac{\lambda_4}{\beta_{16}} + \frac{\theta_4}{\beta_{17}}\right), \quad \text{(A25)}$$

where

$$\alpha_4 = \frac{\gamma_1}{\gamma_2}k_{21,23}Q_{21(23)}\bar{C}_{23}\frac{\alpha_{21}}{\beta_{21}} + \frac{0.7}{\gamma_2}k_{22,31}\bar{C}_{31}\frac{\alpha_{22}}{\beta_{22}} + \frac{\gamma_1^2}{\gamma_2}k_{16,23}\bar{C}_{23}\frac{\alpha_{16}}{\beta_{16}} + \frac{\gamma_1}{\gamma_2}k_{17,31}\bar{C}_{31}\frac{\alpha_{17}}{\beta_{17}}$$

ACPD
10, 15811–15884, 2010

$$+\frac{\gamma_1}{\gamma_2}k_{5,7}Q_{7(5)}\bar{C}_5\frac{\alpha_7}{\beta_7}$$
$$+\frac{1}{\gamma_2}\left(k_{1,24}\bar{C}_1\bar{C}_{24}+\gamma_1 k_{5,24}\bar{C}_5\bar{C}_{24}+\gamma_2 k_{6,24}\bar{C}_6\bar{C}_{24}\right.$$
$$\left.+\gamma_1 k_{5,25}Q_{25(5)}\bar{C}_5\bar{C}_{25}+\gamma_1 k_{5,26}\bar{C}_5\bar{C}_{26}\right), \quad \text{(A26)}$$

$$\beta_4 = \frac{\gamma_1}{\gamma_2}k_{21,23}Q_{21(23)}\bar{C}_{23}\frac{\beta_{21}B_{21}-\alpha_{21}}{\beta_{21}}$$
$$+\frac{0.7}{\gamma_2}k_{22,31}\bar{C}_{31}\frac{\eta_{22}}{\beta_{22}-\beta_{21}}$$
$$+\frac{\gamma_1^2}{\gamma_2}k_{16,23}\bar{C}_{23}\frac{\eta_{16}}{\beta_{16}-\beta_{21}}$$
$$+\frac{\gamma_1}{\gamma_2}k_{17,31}\bar{C}_{31}\frac{\eta_{17}}{\beta_{17}-\beta_{21}}, \quad \text{(A27)}$$

$$\eta_4 = \frac{\gamma_1}{\gamma_2}k_{5,7}Q_{7(5)}\bar{C}_5\frac{\beta_7 B_7-\alpha_7}{\beta_7}, \quad \text{(A28)}$$

$$\delta_4 = \frac{0.7}{\gamma_2}k_{22,31}\bar{C}_{31}\left(B_{22}-\frac{\eta_{22}}{\beta_{22}-\beta_{21}}-\frac{\alpha_{22}}{\beta_{22}}\right), \quad \text{(A29)}$$

$$\lambda_4 = \frac{\gamma_1^2}{\gamma_2}k_{16,23}\bar{C}_{23}\left(B_{16}-\frac{\eta_{16}}{\beta_{16}-\beta_{21}}-\frac{\alpha_{16}}{\beta_{16}}\right)+\frac{\gamma_1}{\gamma_2}k_{17,31}\bar{C}_{31}\cdot\frac{\delta_{17}}{\beta_{17}-\beta_{16}}, \quad \text{(A30)}$$

$$\theta_4 = \frac{\gamma_1}{\gamma_2}k_{17,31}\bar{C}_{31}\left(B_{17}-\frac{\eta_{17}}{\beta_{17}-\beta_{21}}-\frac{\delta_{17}}{\beta_{17}-\beta_{16}}-\frac{\alpha_{17}}{\beta_{17}}\right). \quad \text{(A31)}$$

ACPD
10, 15811–15884, 2010

Acknowledgements. This work was funded by the environmental research program of the Tennessee Valley Authority (TVA) and the Electric Power Research Institute (EPRI). The authors are indebted to the efforts of our colleague, Shandon Smith, who prepared the natural emissions data base used in this project. We are also grateful for the constructive feedback provided by Roger Tanner (TVA) and Eladio Knipping (EPRI) during the course of this work.

References

Atkinson, R., Baulch, D. L., Cox, R. A., Crowley, J. N., Hampson, R. F., Hynes, R. G., Jenkin, M. E., Rossi, M. J., and Troe, J.: Evaluated kinetic and photochemical data for atmospheric chemistry: Volume I - gas phase reactions of O_x, HO_x, NO_x and SO_x species, Atmos. Chem. Phys., 4, 1461–1738, doi:10.5194/acp-4-1461-2004, 2004.

Atkinson, R., Baulch, D. L., Cox, R. A., Crowley, J. N., Hampson, R. F., Hynes, R. G., Jenkin, M. E., Rossi, M. J., Troe, J., and IUPAC Subcommittee: Evaluated kinetic and photochemical data for atmospheric chemistry: Volume II - gas phase reactions of organic species, Atmos. Chem. Phys., 6, 3625–4055, doi:10.5194/acp-6-3625-2006, 2006.

Atkinson, R., Baulch, D. L., Cox, R. A., Crowley, J. N., Hampson, R. F., Hynes, R. G., Jenkin, M. E., Rossi, M. J., and Troe, J.: Evaluated kinetic and photochemical data for atmospheric chemistry: Volume III – gas phase reactions of inorganic halogens, Atmos. Chem. Phys., 7, 981–1191, doi:10.5194/acp-7-981-2007, 2007.

Ayers, G. P. and Gillett, R. W.: DMS and its oxidation products in the remote marine atmosphere: implications for climate and atmospheric chemistry, J. Sea Res., 43, 275–286, 2000.

Behnke, W., George, C., Scheer, V., and Zetzsch, C.: Production and decay of $ClNO_2$ from the reaction of gaseous N_2O_5 with NaCl solution: bulk and aerosol experiments, J. Geophys. Res., 102, 3795–3804, 1997.

Berntsen, T. K. and Isaksen, I. S. A.: A global 3-D chemical transport model for the troposphere: model description and CO and O_3 results, J. Geophys. Res., 102, 21239–21280, 1997.

Berntsen, T. K., Karlsdóttir, S., and Jaffe, D. A.: Influence of Asian emissions on the composition of air reaching the north western United States, Geophys. Res. Lett., 26, 2171–2174, 1999.

Bonifacic, M., Mockel, H., Bahnemann, D., and Asmus, K. D.: Formation of positive-ions and other primary species in oxidation of sulfides by hydroxyl radicals, J. Chem. Soc. Perk. T., 2(7), 675–685, 1975.

ACPD

10, 15811–15884, 2010

Byers, H. R.: Elements of Cloud Physics, The University of Chicago Press, Chicago, 142–146, 1965.
Chawla, O. P. and Fessenden, R. W.: Electron-spin resonance and pulse-radiolysis studies of some reactions of SO_4^-, J. Phys. Chem., 79, 2693–2700, 1975.
De Valk, J. P. J.M.M. and van der Hage, J. C. H.: A model for cloud chemistry processes suitable for use in long range transport models: a sensitivity study, Atmos. Environ., 28, 1653–1663, 1994.
EPA: Guidance for Tracking Progress under the Regional Haze Rule, Office of Air Quality Planning and Standards, Research Triangle Park, NC, EPA-454/B-03–004, 2003.
EPA: Review of the National Ambient Air Quality Standards for Particulate Matter: Policy Assessment of Scientific and Technical Information, Office of Air Quality Planning and Standards, Research Triangle Park, NC, EPA-452/R-05–005, 2005.
Erickson, D. J. III, Seuzaret, C., Keene, W. C., and Gong, S. L.: A general circulation model based calculation of HCl and $ClNO_2$ production from sea salt dechlorination: reactive chlorine emissions inventory, J. Geophys. Res., 104, 8347–8372, 1999.
Ervens, B., Carlton, A. G., Turpin, B. J., Altieri, K. E., Kreidenweis, S. M., and Feingold, G.: Secondary organic aerosol yields from cloud-processing of isoprene oxidation products, Geophys. Res. Lett., 35, doi:10.1029/2007GL031828, 2008.
Finlayson-Pitts, B. J. and Pitts, Jr., J. N.: Chemistry of the Upper and Lower Atmosphere, Academic Press, San Diego, CA, 2000.
Friedl, R. R., Brune, W. H., and Anderson, J. G.: Kinetics of SH with NO_2, O_3, O_2, and H_2O_2, J. Phys. Chem., 89, 5505–5510, 1985.
Gershenzon, M., Davidovits, P., Jayne, J. T., Kolb, C. E., and Worsnop, D. R.: Simultaneous uptake of DMS and ozone on water, J. Phys. Chem. A, 105, 7031–7036, 2001.
Graedel, T. E., Bates, T. S., Bouwman, A. F., Cunnold, D., Dignon, J., Fung, I., Jacob, D. J., Lamb, B. K., Logan, J. A., Marland, G., Middleton, P., Pacyna, J. M., Placet, M., and Veldt, C.: A compilation of inventories of emissions to the atmosphere, Global Biogeochem. Cy., 7, 1–26, 1993.
Grell, G. A., Dudhia, J., and Stauffer, D. R.: A description of the fifth-generation Penn State/NCAR Mesoscale Model (MM5). NCAR Tech. Note, NCAR/TN-398+STR, 122 pp., 1994.
Henze, D. K. and Seinfeld, J. H.: Global secondary organic aerosol from isoprene oxidation, Geophys. Res. Lett., 33, doi:10.1029/2006GL025976, 2006.

ACPD
10, 15811–15884, 2010

Herrmann, H., Ervens, B., Jacobi, H.-W., Wolke, R., Nowacki, P., and Zellner, R.: CAPRAM 2.3: a chemical aqueous phase radical mechanism for tropospheric chemistry, J. Atmos. Chem., 36, 231–284, 2000.

Hoffman, M. R.: On the kinetics and mechanism of oxidation of aquated sulfur-dioxide by ozone, Atmos. Environ., 20, 1145–1154, 1986.

Huie, R. E. and Clifton, C. L.: Temperature-dependence of the rate constants for reactions of the sulfate radical, SO_4^-, with anions, J. Phys. Chem., 94, 8561–8567, 1990.

Jacob, D. J., Park, R., and Logan, J. A.: Documentation and Evaluation of the GEOS-Chem Simulation for 2002 Provided to the VISTAS Group, Harvard University, 2005. (http://vistas-sesarm.org/documents/Harvard_GEOS-CHEM_FinalReport_20050624.doc).

Jourdain, B., Legrand, M., and Preunkert, S.: Multiple year-round atmospheric records of DMS, DMSO, sea-salt and sulfur (MSA and non-sea-salt sulfate) aerosols at Dumont D'Urville (Antarctica) (December 1998–August 2002), EGS-AGU-EUG Joint Assembly, Nice, France, 6–11 April, 2003.

Kaminski, J. W., Neary, L., Struzewska, J., McConnell, J. C., Lupu, A., Jarosz, J., Toyota, K., Gong, S. L., Côté, J., Liu, X., Chance, K., and Richter, A.: GEM-AQ, an on-line global multiscale chemical weather modelling system: model description and evaluation of gas phase chemistry processes, Atmos. Chem. Phys., 8, 3255–3281, doi:10.5194/acp-8-3255-2008, 2008.

Karamchandani, P. and Venkatram, A.: The role of non-precipitating clouds in producing ambient sulfate during summer: results from simulations with the Acid Deposition and Oxidant Model (ADOM), Atmos. Environ., 26A, 1041–1052, 1992.

Knipping, E. M. and Dabdub, D.: Impact of chlorine emissions from sea-salt aerosol on coastal urban ozone, Environ. Sci. Technol., 37, 275–284, 2003.

Koo, B., Chien, C.-J., Tonnesen, G., Morris, R., Johnson, J., Sakulyanontvittaya, T., Piyachaturawat, P., and Yarwood, G.: Natural emissions for regional modeling of background ozone and particulate matter and impacts on emissions control strategies, Atmos. Environ., doi:10.1016/j.atmosenv.2010.02.041, 2010.

Kreidenweis, S. M., Penner, J. E., Yin, F., and Seinfeld, J. H.: The effects of dimethylsulfide upon marine aerosol concentrations, Atmos. Environ., 25A, 2501–2511, 1991.

Kreidenweis, S. M., Walcek, C. J., Feingold, G., Gong, W. M., Jacobson, M. Z., Kim, C. H., Liu, X. H., Penner, J. E., Nenes, A., and Seinfeld, J. H.: Modification of aerosol mass and size distribution due to aqueous-phase SO_2 oxidation in clouds: comparisons of several

ACPD
10, 15811–15884, 2010

models, J. Geophys. Res.-Atmos. 108, 4213, doi:10.1029/2002JD002697, 2003.
Kukui, A., Bossoutrot, V., Laverdet, G., and Le Bras, G.: Mechanism of the reaction of CH_3SO with NO_2 in relation to atmospheric oxidation of dimethyl sulfide: experimental and theoretical study, J. Phys. Chem., 104, 935–946, 2000.
Kukui, A., Borissenko, D., Laverdet, G., and Le Bras, G.: Gas phase reactions of OH radicals with dimethyl sulfoxide and methane sulfinic acid using turbulent flow reactor and chemical ionization mass spectrometry, J. Phys. Chem. A, 107, 5732–5742, 2003.
Lee, Y. N. and Zhou, X. L.: Aqueous reaction-kinetics of ozone and dimethylsulfide and its atmospheric implications, J. Geophys. Res.-Atmos., 99, 3597–3605, 1994.
Levasseur, M., Sharma, S., Cantin, G., Michaud, S., Gosselin, M., and Barrie, L.: Biogenic sulfur emissions from the Gulf of Saint Lawrence and assessment of its impact on the Canadian east coast, J. Geophys. Res., 102(D23), 28025–28039, 1997.
Lin, C.-Y. C., Jacob, D. J., Munger, J. W., and Fiore, A. M.: Increasing background ozone in surface air over the United States, Geophys. Res. Lett., 27, 3465–3468, 2000.
Lucas, D. D., and Prinn, R. G.: Sensitivities of gas-phase dimethylsulfide oxidation products to the assumed mechanisms in a chemical transport model, J. Geophys. Res., 110, D21312, doi:10.1029/2004JD005386, 2005.
Möller, D. and Mauersberger, G.: Cloud chemistry effects on tropospheric photooxidants in polluted atmosphere – model results, J. Atmos. Chem., 14, 153–165, 1992.
Morris, R. E., Koo, B., Guenther, A., Yarwood, G., McNally, D., Tesche, T. W., Tonnesen, G., Boylan, J., and Brewer, P.: Model sensitivity evaluation for organic carbon using two multi-pollutant air quality models that simulate regional haze in the southeastern United States, Atmos. Environ., 40, 4960–4972, 2006.
Mueller, S. F., Bailey, E. M., Cook, T. M., and Mao, Q.: Treatment of clouds and the associated response of atmospheric sulfur in the Community Multiscale Air Quality (CMAQ) modeling system, Atmos. Environ., 40, 6804–6820, 2006.
National Aeronautics and Space Administration: Chemical Kinetics and Photochemical Data for Use in Stratospheric Modeling – Evaluation Number 12, Jet Propulsion Laboratory, Publication 97–4, 266 pp., 1997 (http://ntrs.nasa.gov/archive/nasa/casi.ntrs.nasa.gov/19970037557_1997085720.pdf).
National Acid Precipitation Assessment Program: The Regional Acidic Deposition Model and Engineering Model, Report 4. in: Acid Deposition: State of Science and Technology, ed. by: Irving P. M., Vol. 1, Emissions, Atmospheric Processes, and Deposition, Office of the

ACPD
10, 15811–15884, 2010

Director, Washington, DC, 67–69, 1991.
Oltmans, S. J., Lefohn, A. S., Harris, J. M., and Shadwick, D. S.: Background ozone levels of air entering the west coast of the US and assessment of longer-term changes, Atmos. Environ., 42, 6020–6038, 2008.
Park, R. J., Jacob, D. J., Field, B. D., and Yantosca, R. M.: Natural and transboundary pollution influences on sulfate-nitrate-ammonium aerosols in the United States: implications for policy, J. Geophys. Res., 109, D15205, doi:10.1029/2003JD004473, 2004.
Pickering, K. E., Wang, Y., Tao, W.-K., Price, C., and Müller, J.-F.: Vertical distributions of lightning NO_x for use in regional and global chemical transport models, J. Geophys. Res., 103, 31,203–31,216, 1993.
Sciare, J., Baboukas, E., and Mihalopoulos, N.: Short-term variability of atmospheric DMS and its oxidation products at Amsterdam Island during summer time, J. Atmos. Chem., 39, doi:10.1023/A:1010631305307, 2001.
Sciare, J., Kanakidou, M., and Mihalopoulos, N.: Diurnal and seasonal variation of atmospheric dimethylsulfoxide at Amsterdam Island in the southern Indian Ocean, J. Geophys. Res., 105(D13), 17257–17265, 2000.
Seinfeld, J. H. and Pandis, S. N.: Atmospheric Chemistry and Physics, John Wiley & Sons, New York, 627–634, 1998.
Smith, S. N. and Mueller, S. F.: Modeling natural emissions in the Community Multiscale Air Quality (CMAQ) Model–I: building an emissions data base, Atmos. Chem. Phys., 10, 4931–4952, doi:10.5194/acp-10-4931-2010, 2010.
Tanaka, P. L. and Allen, D. T.: Incorporation of chlorine reactions into the carbon bond-IV mechanism: mechanism updates and preliminary performance evaluation, report on contract no. 9880077600-18 between the University of Texas and the Texas Natural Resource Conservation Commission, Center for Energy and Environmental Resources, University of Texas, Austin, TX, 2001.
Tesche, T. W., Morris, R., Tonnesen, G., McNally, D., Boylan, J., and Brewer, P.: CMAQ/CAMx annual 2002 performance evaluation over the eastern US, Atmos. Environ., 40, 4906–4919, 2008.
Van den Berg, A. R., Dentener, F. J., and Lelieveld, J.: Modelling the chemistry of the marine boundary layer; sulphate formation and the role of sea salt aerosol particles, J. Geophys. Res., 105, 11671–11698, 2000.
Vingarzan, R.: A review of surface ozone background levels and trends, Atmos. Environ., 38,

ACPD
10, 15811–15884, 2010

3431–3442, 2004.
Watts, S. F., Watson, A., and Brimblecombe, P.: Measurements of the aerosol concentrations of methanesulphonic acid, dimethyl sulphoxide and dimethyl sulphone in the marine atmosphere of the British Isles, Atmos. Environ., 21, 2667–2672, 1987.
Williams, J. E., Dentener, F. J., and van den Berg, A. R.: The influence of cloud chemistry on HO_x and NO_x in the moderately polluted marine boundary layer: a 1-D modelling study, Atmos. Chem. Phys., 2, 39-54, doi:10.5194/acp-2-39-2002, 2002.
Yang, G.-P., Zhang, H.-H., Su, L.-P., and Zhou, L.-M.: Biogenic emission of dimethylsulfide (DMS) from the North Yellow Sea, China and its contribution to sulfate in aerosol during summer, Atmos. Environ., 43, 2196–2203, 2009.
Yarwood, G., Rao, S., Yocke, M., and Whitten, G.: Updates to the Carbon Bond Chemical Mechanism: CB05. Report to the US EPA, RT-0400675, 2005 (http://www.camx.com/publ/pdfs/CB05_Final_Report_120805.pdf).
Yin, F., Grosjean, D., and Seinfeld, J. H.: Photooxidation of dimethyl sulfide and dimethyl disulfide. I: mechanism development, J. Atmos. Chem., 11, 309–364, 1990.
Yvon, S. A. and Saltzman, E. S.: Atmospheric sulfur cycling in the tropical Pacific marine boundary layer (12° S, 135° W): a comparison of field data and model results 2. sulfur dioxide, J. Geophys. Res., 101(D3), 6911–6918, 1996.
Zaveri, R. A: Development and Evaluation of a Comprehensive Tropospheric Chemistry Model for Regional and Global Applications, Ph.D. dissertation, Virginia Polytechnic Institute and State University, 250 pp., 1997.
Zhu, L.: Aqueous Phase Reaction Kinetics of Organic Sulfur Compounds of Atmospheric Interest, Ph.D. dissertation, School of Earth and Atmospheric Sciences, Georgia Institute of Technology, 261 pp., 2004.
Zhu, L., Nenes, A., Wine, P. H., and Nicovich, J. M.: Effects of aqueous organosulfur chemistry on particulate methanesulfonate to non-sea salt sulfate ratios in the marine atmosphere, J. Geophys. Res., 111, D05316. doi:10.1029/2005JD006326, 2006.

ACPD
10, 15811–15884, 2010

Table 1. Chlorine reactions added to CB05 in CMAQ4.6.[a]

Reaction[b]	Rate constant[c], k (cm^3 $molecule^{-1}$ s^{-1})
$Cl_2+h\nu \rightarrow 2Cl$	$0.264k_{NO_2}$
$HOCl+h\nu \rightarrow OH+Cl$	$0.51k_{ACRO}$
$PAR+Cl \rightarrow HCl+0.87XO_2+0.13XO2N+0.11HO_2+0.11ALD2+0.76ROR-0.11PAR$	$78k_{OH+PAR}$
$OLE+Cl \rightarrow FMCL+ALD2+2XO_2+HO_2-PAR$	$20k_{OH+OLE}$
$CH_4+Cl \rightarrow HCl+XO_2+HCHO+HO_2$	$6.6\times10^{-12}\exp(-1240/T)$
$ETH+Cl \rightarrow 2XO_2+HCHO+FMCL+HO_2$	$12.6k_{OH+ETH}$
$ISOP+Cl \rightarrow 0.15HCl+XO_2+HO_2+0.28ICL1$	$4.5k_{OH+ISOP}$
$ICL1+OH \rightarrow ICL2$	$0.19k_{OH+ISOP}$
$Cl+O_3 \rightarrow ClO+O_2$	$2.9\times10^{-11}\exp(-260/T)$
$ClO+NO \rightarrow Cl+NO_2$	$6.2\times10^{-12}\exp(295/T)$
$ClO+HO_2 \rightarrow HOCl+O_2$	$4.6\times10^{-13}\exp(710/T)$
$ClNO_2+OH \rightarrow HOCl+NO_2$	$2.4\times10^{-12}\exp(-1250/T)$

[a] All but the last reaction are based on Tanaka and Allen (2001). The reaction of $ClNO_2$ with OH is from Atkinson et al. (2007).

[b] CMAQ species abbreviations: ACRO=acrolein (in reference to the SAPRC99 mechanism); PAR=paraffin lumped group; OLE=olefin lumped group; ETH=ethene; ISOP=isoprene; XO2N=NO converted to organic nitrate; ALD2=acetaldehyde carbonyl lumped group; ROR=secondary alkoxy radical; FMCL=formyl chloride; ICL1=1-chloro-3-methyl-3-butene-2-one; ICL2=derivative of ICL1.

[c] Constants that are defined in terms of other rate constants are denoted with "$nk_{reaction}$" where "reaction" denotes a pre-existing CMAQ chemical or photolysis rate constant with n proportionality factor.

ACPD
10, 15811–15884, 2010

Table 2. Reactions added to CB05 for inorganic sulfur species and their reaction products.

Reactants	Products	Rate constant (cm^3 $molecule^{-1}$ s^{-1})	Reference
H_2S+OH	$SH+H_2O$	$6.0\times10^{-12}\exp(-80/T)$	Atkinson et al., 2004
H_2S+NO_3	$SH+HNO_3$	1.0×10^{-15}	Atkinson et al., 2004
H_2S+Cl	$SH+HCl$	$3.7\times10^{-11}\exp(208/T)$	Atkinson et al., 2004
$SH+O$	$SO+H$	1.6×10^{-10}	NASA, 1997
$SH+O_2$	$SO+OH$	4.0×10^{-19}	NASA, 1997
$SH+O_3$	$HSO+O_2$	$9.5\times10^{-12}\exp(-280/T)$	Atkinson et al., 2004
$SH+NO_2$	$HSO+NO$	$2.9\times10^{-11}\exp(240/T)$	Atkinson et al., 2004
$SH+NO+M$	$HSNO+M$	$k_0=2.4\times10^{-31}(T/300)^{-3}$[M] $k_\infty=2.7\times10^{-11}$ [a]	Atkinson et al., 2004
$SH+Cl_2$	$ClSH+Cl$	$1.7\times10^{-11}\exp(690/T)$	NASA, 1997
$HSO+NO_2$	HSO_2+NO	9.6×10^{-12}	NASA, 1997
$HSO+O_2$	HSO_2+O	2.0×10^{-17}	Atkinson et al., 2004
$HSO+O_3$	HSO_2+O_2	1.1×10^{-13}	Atkinson et al., 2004
$SO+OH$	SO_2+H	8.6×10^{-11}	NASA, 1997
$SO+O_2$	SO_2+O	$1.6\times10^{-13}\exp(-2280/T)$	Atkinson et al., 2004
$SO+O_3$	SO_2+O_2	$4.5\times10^{-12}\exp(-1170/T)$	Atkinson et al., 2004
$SO+NO_2$	SO_2+NO	1.4×10^{-11}	Atkinson et al., 2004
$SO+ClO$	SO_2+Cl	2.8×10^{-11}	NASA, 1997
HSO_2+O_2	HO_2+SO_2	3.0×10^{-13}	NASA, 1997

[a] Termolecular rate constant expression:
$k=\left[\frac{k_0}{1+(k_0/k_\infty)}\right]0.6^{(1+[\log_{10}(k_0/k_\infty)]^2)^{-1}}$

ACPD
10, 15811–15884, 2010

Table 3. Reactions added to CB05 for organic sulfur species and their reaction products.[a]

Reactants	Products	Rate constant (cm^3 $molecule^{-1}$ s^{-1})[b]	Reference
DMS+O	$MSO+CH_3$	$1.34\times10^{-11}\exp(409/T)$	Atkinson et al., 2004
$DMS+NO_3$	$MSCH_2+HNO_3$	$1.9\times10^{-13}\exp(520/T)$	Atkinson et al., 2004
DMS+OH	$MSCH_2+H_2O$	$1.1\times10^{-11}\exp(-253/T)$	Atkinson et al., 2004
$DMS+OH+O_2$	0.5DMSO+0.2DMSO2+0.3MSIA	$\{1\times10^{-39}\exp(5820/T)[O_2]\}/\{1+5\times10^{-30}\exp(6280/T)[O_2]\}$	Zhu et al., 2006
DMS+Cl	$MSCH_2+HCl$	3.3×10^{-10}	Atkinson et al., 2004
$MSCH_2+O_2+M$	MSP+M	5.7×10^{-12}	Finlayson-Pitts and Pitts, 2000; Atkinson et al., 2004
$MSCH_2+NO_3$	MSP+NO	3.0×10^{-10}	NASA, 1997
MSP+NO	$CH_3S+HCHO+NO_2$	$4.9\times10^{-12}\exp(260/T)$	Atkinson et al., 2004; Zhu et al., 2006
MSP+MSP	$2CH_3S+2HCHO+O_2$	1.0×10^{-11}	Atkinson et al., 2004; Zhu et al., 2006
$MSP+HO_2$	$CH_3S+HCHO+OH+O_2$	$3.8\times10^{-13}\exp(780/T)$	Zhu et al., 2006; following Tyndall et al., 2001
CH_3S+O_3	$0.9SO_2+0.1H_2SO_4+0.9CH_3O+0.1CH_3$[c]	$1.15\times10^{-12}\exp(430/T)$[d]	Atkinson et al., 2004; Zhu et al., 2006
CH_3S+NO_2	MSO+NO	$3.0\times10^{-11}\exp(210/T)$	Atkinson et al., 2004
$MSO+O_3$	$0.14CH_3S+0.86CH_3+0.86SO_2+O_2$	6.0×10^{-13}	Finlayson-Pitts and Pitts, 2000; Atkinson et al., 2004
$MSO+NO_2$	CH_3+SO_2+NO	1.2×10^{-11}	Finlayson-Pitts and Pitts, 2000; Atkinson et al., 2004
DMSO+OH	0.9MSIA+0.1DMSO2	9.0×10^{-11}	Kukui et al., 2003; Zhu et al., 2006
MSIA+OH	$0.9SO_2+0.1MSA$	9.0×10^{-11}	Kukui et al., 2003; Zhu et al., 2006
CH_3+O_3	CH_3O+O_2	$4.7\times10^{-12}\exp(-210/T)$	Atkinson et al., 2004, 2006
CH_3+O	HCHO+H	1.3×10^{-10}	Atkinson et al., 2006
CH_3O+O_2	$HCHO+HO_2$	$7.2\times10^{-14}\exp(-1080/T)$	Atkinson et al., 2004, 2006
CH_3O+NO_2	HCHO+HONO	$9.6\times10^{-12}\exp(-1150/T)$	Atkinson et al., 2004, 2006

[a] Abbreviations: DMS=dimethylsulfide, CH_3SCH_3; DMSO=dimethylsulfoxide, $CH_3S(O)CH_3$; DMSO2=dimethylsulfone, $CH_3S(O)(O)CH_3$; $MSCH_2$=methylthiomethyl radical, CH_3SCH_2; MSP=methylthiomethylperoxyl radical, CH_3SCH_2OO; MSO=methylsulfoxide radical, CH_3SO; MSIA=methanesulfinic acid, CH_3SOOH; MSA=methanesulfonic acid, $CH_3S(O)(O)OH$.

[b] The exception is for termolecular rate constants that have units of cm^6 $molecule^{-2}$ s^{-1}.

[c] The mechanism of Zhu et al. (2006) treats the reaction of CH_3S with a variety of species as one reaction producing sulfur dioxide and sulfuric acid with no additional products specified. As implemented in CMAQ, the additional products are assumed to be species needed to achieve stoichiometric closure to the reaction in the presence of H_2O.

[d] This is believed to be a termolecular reaction (Atkinson et al., 2004) but the rate constant at different pressures has not been determined. See Sect. 3.1.4 for more information.

ACPD
10, 15811–15884, 2010

Table 4. Airborne chemical species ingested by clouds and used to compute droplet acidity.

Species	CMAQ cloud module	
	Original (version 4.6)	Revised
H_2SO_4 (gas)	X	X
SO_2 (gas)	X	X
H_2O_2 (gas)	X	X
CO_2 (gas)	X	X
NH_3 (gas)	X	X
MSIA (gas)		X
MSA (gas)		X
HCl (gas)	X	X
HNO_3 (gas)	X	X
H_2CO_2 (gas)	X	X
NaCl (aerosol)	X	X
KCl (aerosol)	X	X
$CaCl_2$ (aerosol)	X	X
$MgCl_2$ (aerosol)	X	X
NH_3NO_3 (aerosol)	X	X

ACPD
10, 15811–15884, 2010

Table 5. Revised set of heterogeneous cloud reactions in CMAQ4.6.[a]

Reaction[b]	Rate constant, k ($M^{-1}\ s^{-1}$)
$DMS+O_3 \rightarrow DMSO+O_2$	$5.3\times10^{12}\exp(-2600/T)$ [c]
$DMS+OH \rightarrow DMSO+HO_2$	1.9×10^{10} [d]
$DMSO+O_3 \rightarrow DMSO2+O_2$	5.7×10^{0} [e]
$DMSO+OH \rightarrow MSIA+CH_3$	$4.7\times10^{11}\exp(-1270/T)$ [f]
$DMSO+SO_4^- \rightarrow CH_3SO_2^-+SO_4^{2-}+2H^+$	$3.7\times10^{11}\exp(-1440/T)$ [f]
$DMSO+Cl \rightarrow CH_3SO_2^-+2H^++Cl^-$	6.3×10^{9} [f]
$DMSO+Cl_2^- \rightarrow CH_3SO_2^-+Cl_2$	1.7×10^{7} [f]
$DMSO2+OH \rightarrow 0.3MSA+0.7SO_4^{2-}+1.4H^+$	$5.1\times10^{9}\exp(-1690/T)$ [f]
$CH_3SO_2^-+OH \rightarrow CH_3SO_3^-+H^++O_2^-$	7.7×10^{9} [f]
$CH_3SO_2^-+SO_4^- \rightarrow CH_3SO_3^-+SO_4^{2-}+H^+$	1.0×10^{9} [f]
$CH_3SO_2^-+Cl_2^- \rightarrow CH_3SO_3^-+2Cl^-+H^+$	8.0×10^{8} [f]
$CH_3SO_3^-+OH \rightarrow SO_4^{2-}+H^+$	$8.8\times10^{10}\exp(-2630/T)$ [f]
$SO_2+O_3 \rightarrow SO_4^{2-}+2H^+$	2.4×10^{4} [g]
$HSO_3^-+O_3 \rightarrow SO_4^{2-}+H^+$	$3.5\times10^{5}\exp[-5530(1/T-1/298)]$ [h]
$SO_3^{2-}+O_3 \rightarrow SO_4^{2-}$	$1.5\times10^{9}\exp[-5280(1/T-1/298)]$ [h]
$HSO_3^-+H_2O_2 \rightarrow SO_4^{2-}+H^+$	$\frac{7.45\times10^{7}\exp[-4430(1/T-1/298)]}{1+13[H^+]}$ [h]
$HSO_3^-+MHP \rightarrow SO_4^{2-}+H^+$	$1.75\times10^{7}\exp[-3801(1/T-1/298)]$
$HSO_3^-+PAA \rightarrow SO_4^{2-}+H^+$	$3.64\times10^{7}\{[H^+]+1.65\times10^{-5}\}\exp[-3994(1/T-1/298)]$

[a] CMAQ species abbreviations: MHP=methylhydrogen peroxide; PAA=peroxyacetyl acid.
[b] The last six reactions are essentially those treated in the standard version of CMAQ, although their rate constants were taken from other sources except for the last two which are the expressions for k used in CMAQ.
[c] Zhu (2004), Zhu et al. (2006), Gershenzon et al. (2001).
[d] Zhu (2004), Zhu et al. (2006), Bonifacic et al. (1975).
[e] Zhu (2004), Zhu et al. (2006), Lee and Zhou (1994).
[f] Zhu (2004), Zhu et al. (2006).
[g] Zhu (2004), Zhu et al. (2006), Kreidenweis et al. (2003).
[h] Zhu (2004), Zhu et al. (2006), Hoffman (1986), Kreidenweis et al. (2003).

ACPD
10, 15811–15884, 2010

Table 6. Species treated in the revised CMAQ cloud module.

Index number[a]	Species	Steady-state	Reactive	Likely to be non-uniform
1	SO_2	X	X	
2	H_2SO_4	X		
3	HSO_4^-	X		
4	SO_4^{2-}			
5	HSO_3^-	X	X	
6	SO_3^{2-}	X	X	
7	H_2O_2		X	X
8	HO_2^-	[b]		
9	CO_2	X		
10	HCO_3^-	X		
11	H^+	X		
12	CO_3^{2-}	X		
13	NH_3	X		
14	NH_4^+	X		
15	OH^-	X		
16	$CH_3SO_2^-$		X	
17	$CH_3SO_3^-$		X	
18	MSIA		[c]	
19	MSA		[c]	
20	DMS	X	X	X
21	DMSO		X	X
22	DMSO2		X	
23	SO_4^-	X	X	
24	O_3	X	X	
25	MHP	X	X	X
26	PAA	X	X	
27	HCl	X		
28	Cl^-	X		
29	HNO_3	X		
30	NO_3^-	X		
31	OH	X	X	
32	Cl	X	X	
33	Cl_2^-	X	X	
34	Na^+	X		
35	K^+	X		
36	Mg^{2+}	X		
37	Ca^{2+}	X		

[a] Used as a subscript to identify species in the transient equations.
[b] Although linked to a species that is not steady-state, the activity of this species is only determined for the purpose of computing the initial equilibrium cloud droplet acidity.
[c] These species are not themselves reactive but dissociate to ions that are reactive.

ACPD
10, 15811–15884, 2010

Table 7. Average simulated winter and summer natural pollutant levels for the modeling domain.

Pollutant	Winter (Dec–Feb)	Summer (Jun–Aug)
Ozone (ppbV)	27.3	23.5
Ammonium+sulfate[a] ($\mu g\,m^{-3}$)	0.12	0.27
Ammonium nitrate[a] ($\mu g\,m^{-3}$)	0.01	0.02
Organic carbon[a] ($\mu g\,m^{-3}$)	0.35	2.22
Elemental carbon[a] ($\mu g\,m^{-3}$)	0.004	0.23
Windblown dust[a] ($\mu g\,m^{-3}$)	0.12	0.14
Sea salt[a] ($\mu g\,m^{-3}$)	0.02	0.02
Total $PM_{2.5}$[b] ($\mu g\,m^{-3}$)	0.91	4.66
PM_c ($\mu g\,m^{-3}$)	1.69	1.05

[a] In the fine particle size fraction (i.e., below 2.5 µm).
[b] Assumes organic aerosol mass equal to 1.8∗OC.

ACPD
10, 15811–15884, 2010

Table 8. CMAQ configurations and assumptions used in model test simulations.

Test	CMAQ Configuration and Assumptions[a]
A	Unmodified CMAQ4.6 using CB05 mechanism
B	Test A configuration with CB05 mechanism modified to include DMS and H_2S gas phase chemistry
C	Test B configuration with standard cloud module replaced by module that includes organic sulfur chemistry
D	Test C configuration but with OH cloud uptake blocked
E	Test C configuration but with Pacific Ocean clouds enhanced between 250 and 750 m[b]
F	Test C configuration with α=0.001 [c]

[a] All tests were run for the entire month of June.
[b] All model layers in 250–750 m range included clouds with minimum cloud water content of 0.5 g m^{-3}.
[c] The proportion, α, of $[HSO_3^-]_{aq}+[HSO_4^-]_{aq}$ in cloud droplets that is assumed to convert to the sulfate radical, SO_4^-. All other tests assumed $\alpha=1\times10^{-6}$.

ACPD
10, 15811–15884, 2010

Table 9. Modified CMAQ4.6 simulated levels of sulfur compounds in the marine boundary layer compared with values from other sources.

Species	Metric[a]	CMAQ[b] Test C	CMAQ[b] Test F	Measured[c]	Citation source
DMS	nanomoles m^{-3}	10	9	5	Yang et al. (2009)
	pptV	250	225	300	Yvon and Saltzman (1996), Levasseur et al. (1997), Ayers and Gillett (2000), Sciare et al. (2001), Jourdain et al. (2003)
DMSO	pptV	2	1.1	5	Sciare et al. (2000), Sciare et al. (2001), Jourdain et al. (2003)
MSA[d]	nanomoles m^{-3}	0.3–0.4	0.5–0.6	2.8	Watts et al. (1987), Yang et al. (2009)
	pptV	8–10	13–15	20	Ayers and Gillett (2000), Sciare et al. (2001), Jourdain et al. (2003)
SO_2	pptV	19	18	114	Sciare et al. (2001)
Sulfate	$\mu g\, m^{-3}$	0.3	0.4	8	Yang et al. (2009)
	pptV	90	100	70	Yvon and Saltzman (1996), Sciare et al. (2001), Jourdain et al. (2003)

[a] Maximum mass concentrations and mixing ratios do not usually occur in the same locations or at the same times.
[b] Average for June 2002 over the Pacific Ocean portion of the modeling domain.
[c] Averages over multiple samples, locations and seasons.
[d] It is not clear to what extent MSIA contributes to measured values of MSA given the similarities in the two species and the fact that MSIA can convert to MSA in aqueous solution. Model results presented here include a range of values that reflect this uncertainty and the fact that the model makes a clear distinction between the two S_{org} components.

ACPD
10, 15811–15884, 2010

Table A1. Index list for aqueous species included in the revised cloud chemistry module.[a]

Species	Index	Species	Index
SO_2	1	DMS	20
H_2SO_4	2	DMSO	21
HSO_4^-	3	DMSO2	22
SO_4^{2-}	4	SO_4^-	23
HSO_3^-	5	O_3	24
SO_3^{2-}	6	MHP	25
H_2O_2	7	PAA	26
HO_2^-	8	HCl	27
CO_2	9	Cl^-	28
HCO_3^-	10	HNO_3	29
H^+	11	NO_3^-	30
CO_3^{2-}	12	OH	31
NH_3	13	Cl	32
NH_4^+	14	Cl_2^-	33
OH^-	15	Na^+	34
$CH_3SO_2^-$	16	K^+	35
$CH_3SO_3^-$	17	Mg^{2+}	36
MSIA	18	Ca^{2+}	37
MSA	19		

[a] Abbreviations: DMS=dimethylsulfide, DMSO=dimethylsulfoxide, DMSO2=dimethylsulfone, MSIA=methanesulfinic acid, MSA=methanesulfonic acid, MHP=methylhydrogen peroxide, PAA=peroxyacetic acid

ACPD
10, 15811–15884, 2010

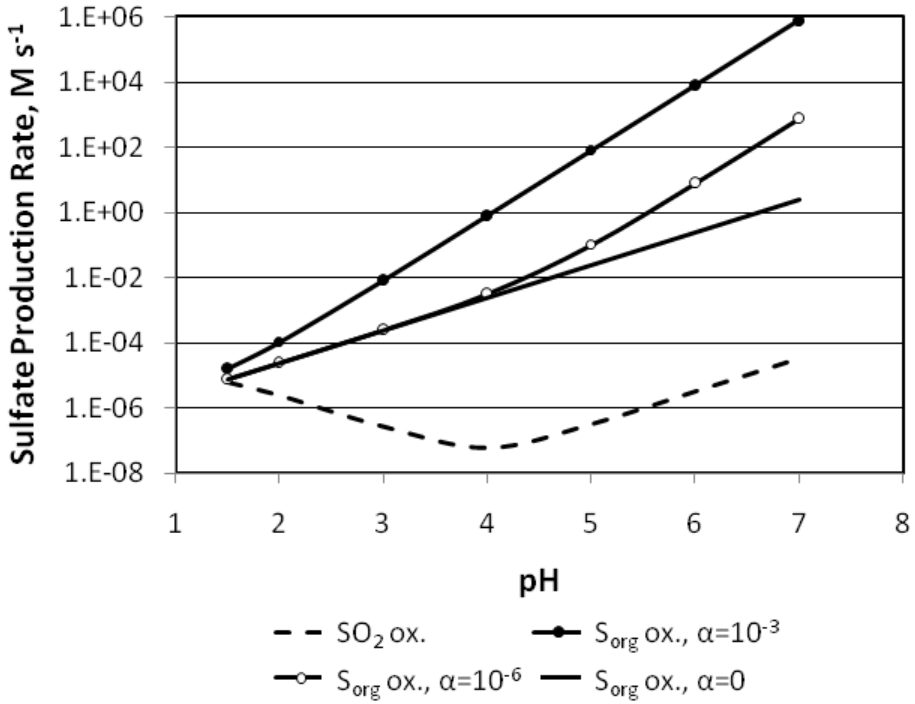

Fig. 1. Comparative steady-state heterogeneous sulfate formation rates in the presence of SO_2 and equal parts DMSO and DMSO2 for different levels of $[SO_4^-]_{(aq)}$ as determined from the parameter α. Atmospheric conditions are: 298 K, 1 atm, 0.5 µg m^{-3} cloud liquid water content, X_{SO_2}=0.4 ppbV, X_{DMSO}=0.2 ppbV, X_{DMSO_2}=0.2 ppbV, X_{O_3}=30 ppbV, $X_{OH}=1\times10^{-10}$ ppbV, total peroxide=0.3 ppbV.

ACPD
10, 15811–15884, 2010

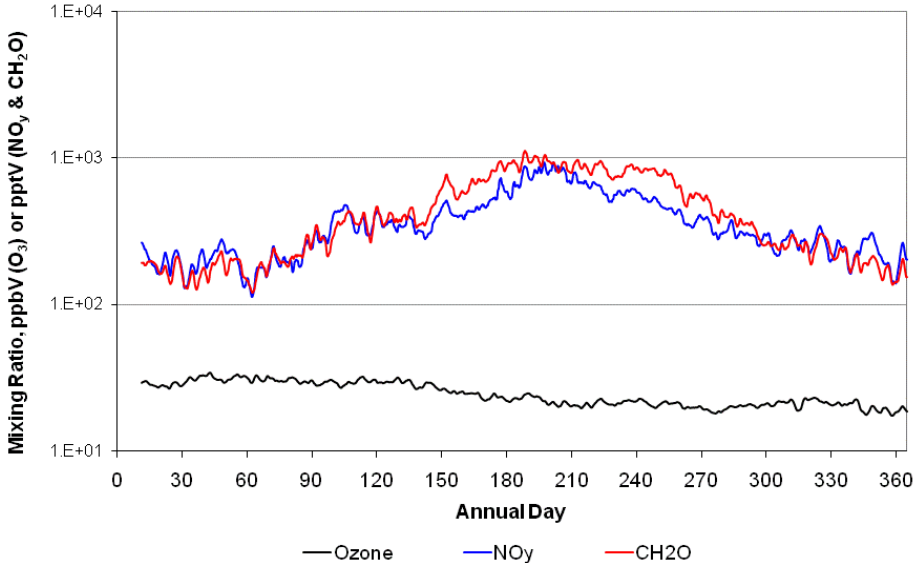

Fig. 2. Grid-averaged time series of three photochemically active species for the natural emissions simulation of 2002. Diurnal noise was removed by applying a 24-h averaging filter.

ACPD
10, 15811–15884, 2010

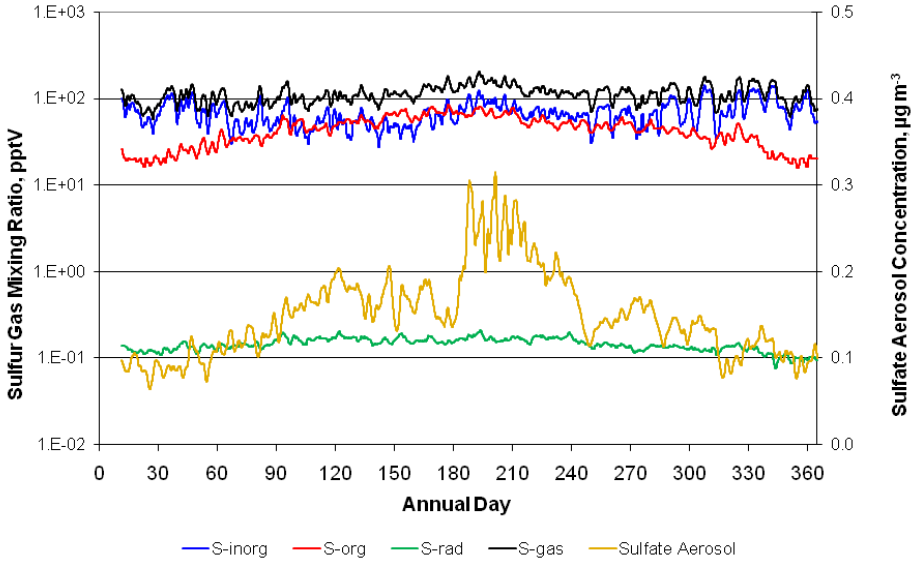

Fig. 3. Grid-averaged time series of various gas and aerosol sulfur species for the natural emissions simulation of 2002. Diurnal noise was removed by applying a 24-h averaging filter.

ACPD
10, 15811–15884, 2010

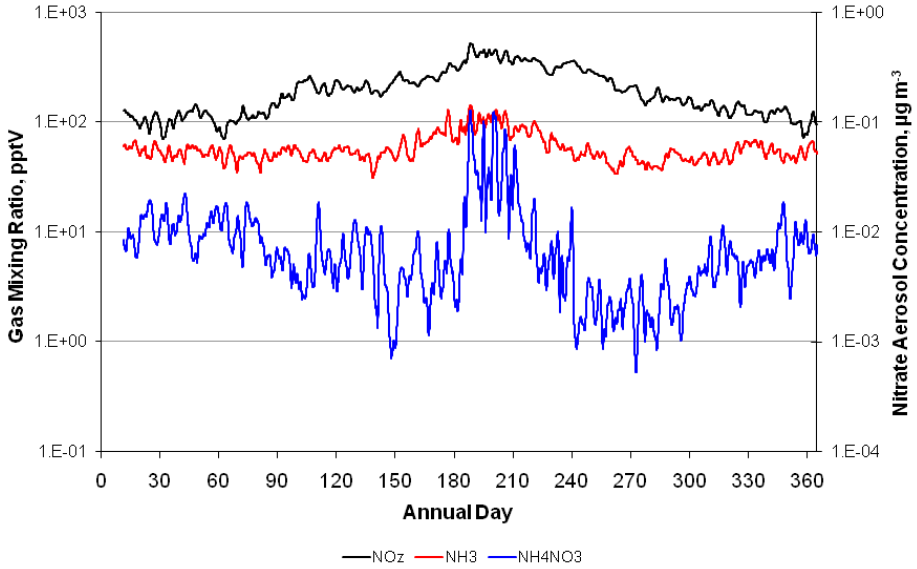

Fig. 4. Grid-averaged time series of NO_z, NH_3 and ammonium nitrate aerosol for the natural emissions simulation of 2002. Diurnal noise was removed by applying a 24-h averaging filter.

ACPD
10, 15811–15884, 2010

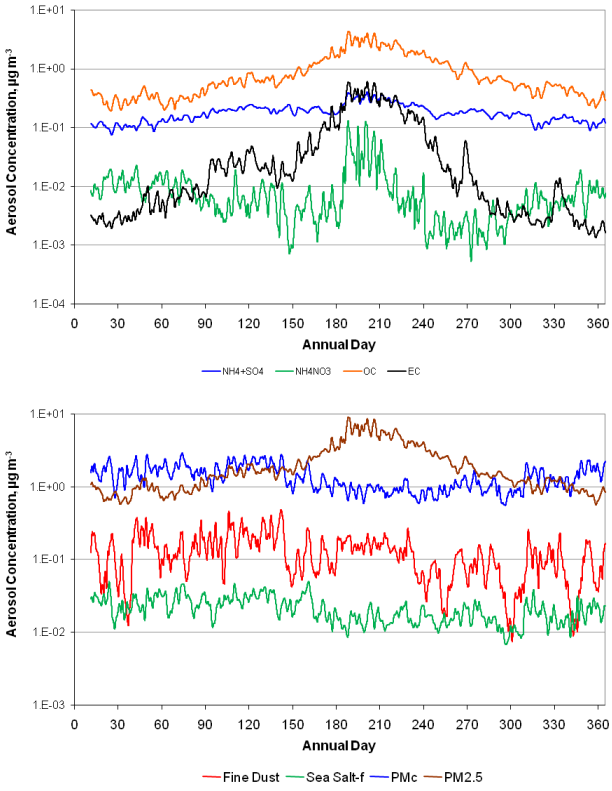

Fig. 5. Grid-averaged time series of simulated particle concentrations for the natural emissions simulation of 2002. Diurnal noise was removed by applying a 24-h averaging filter.

ACPD
10, 15811–15884, 2010

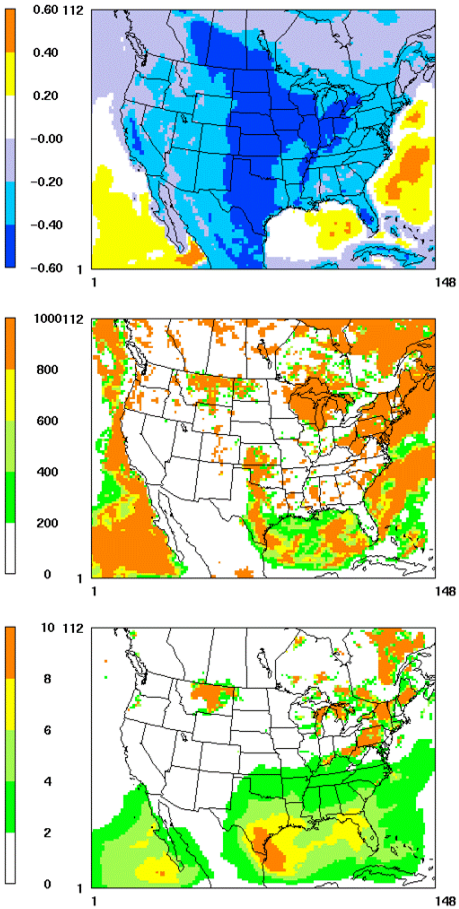

Fig. 6. Mean simulated relative changes, $\bar{\Delta}$, during June in natural levels of airborne pollutants (top: OH; middle: SO_2; bottom: aerosol sulfate) due to the introduction of reduced sulfur and chlorine gas chemistry into CMAQ4.6 (i.e., test B changes relative to test A). Model output is for the surface layer.

ACPD
10, 15811–15884, 2010

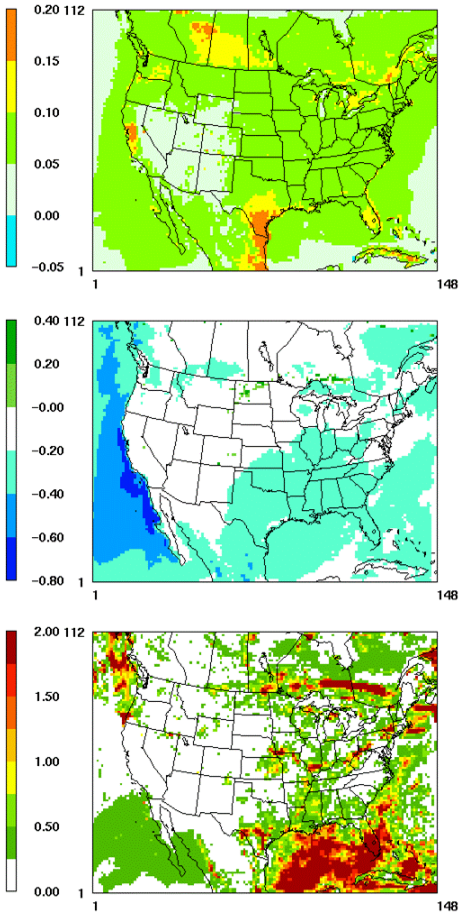

Fig. 7. Same as in Fig. 6 except the changes represent the impacts from adding organic sulfur chemistry to the cloud chemistry module (i.e., test C changes relative to test B).

ACPD
10, 15811–15884, 2010

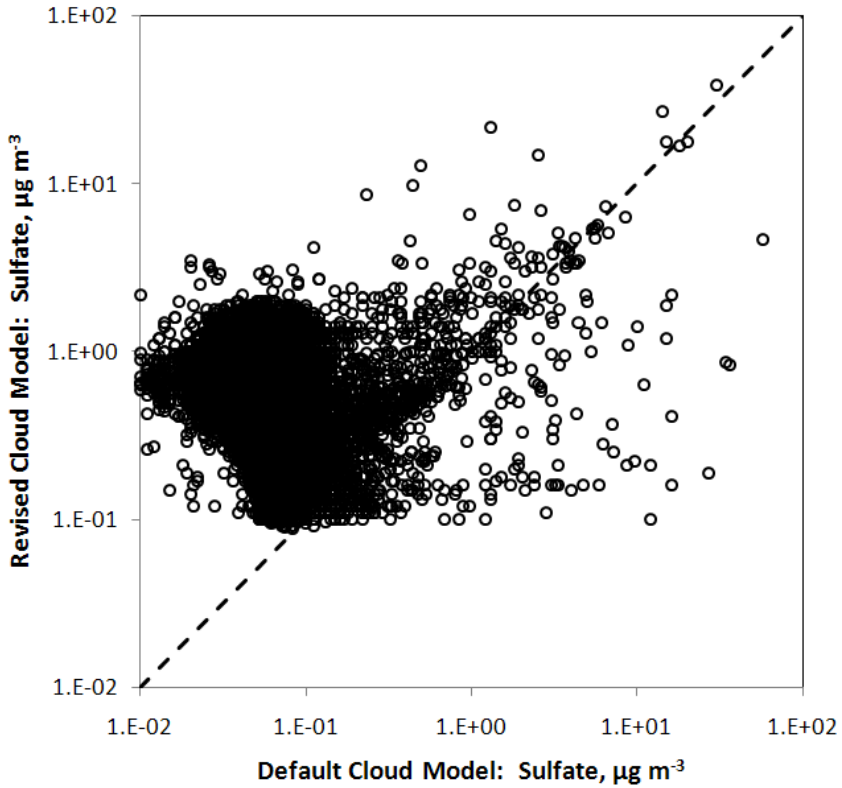

Fig. 8. Comparison of CMAQ hourly sulfate aerosol mass concentrations in the surface layer using the revised (with S_{org} chemistry turned off) and default (original) cloud chemistry models. The new cloud model produces lower values for some of the higher original cases and higher values for most of the lower original cases. Model differences are a result of differences in the treatment of gaseous reactant uptake by cloud droplets and the timing of cloud and gas-phase chemistry.

ACPD
10, 15811–15884, 2010

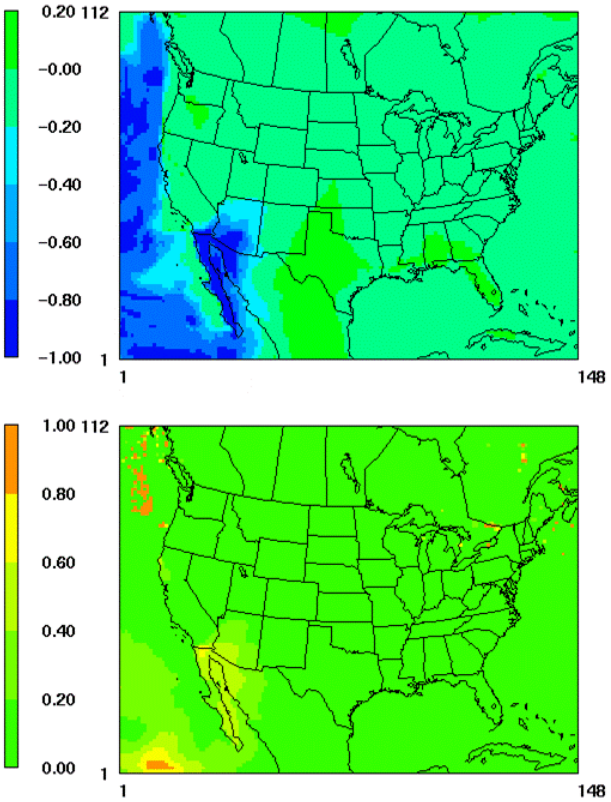

Fig. 9. Average relative changes ($\bar{\Delta}$) for June in surface layer SO_2 mixing ratio (top) and sulfate concentration (bottom) incurred by enhancing cloud cover over the Pacific Ocean portion of the modeling domain (i.e., test E). The reference case is test C.

ACPD
10, 15811–15884, 2010

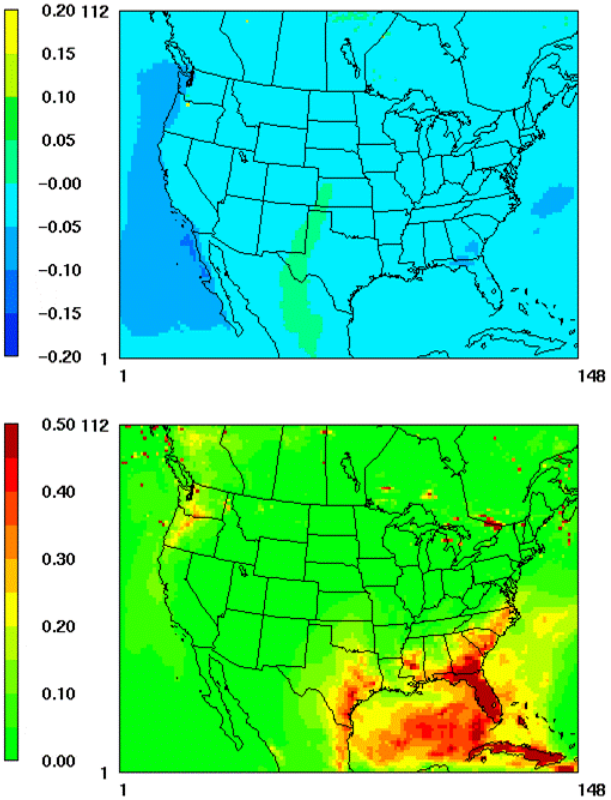

Fig. 10. Average relative changes ($\bar{\Delta}$) for June in surface layer SO_2 mixing ratio (top) and sulfate concentration (bottom) incurred by increasing the fraction of sulfate radical formed from aqueous SO_2 and H_2SO_4 in clouds (i.e., test F). The reference case is test E results.

ACPD
10, 15811–15884, 2010